www.sciencemag.org/content/353/6302/929/suppl/DC1

Supplementary Material for

pVHL suppresses kinase activity of Akt in a proline-hydroxylation–dependent manner

Jianping Guo, Abhishek A. Chakraborty, Pengda Liu, Wenjian Gan, Xingnan Zheng, Hiroyuki Inuzuka, Bin Wang, Jinfang Zhang, Linli Zhang, Min Yuan, Jesse Novak, Jin Q. Cheng, Alex Toker, Sabina Signoretti, Qing Zhang, John M. Asara, William G. Kaelin Jr., Wenyi Wei*

*Corresponding author. E-mail: wwei2@bidmc.harvard.edu

Published 26 August 2016, *Science* **353**, 929 (2016)
DOI: 10.1126/science.aad5755

This PDF file includes:

Materials and Methods

Cell culture and transfection

HEK293, 293T, HeLa, U2OS, renal carcinoma cell lines including *VHL*-deficient cells (RCC4 and 786-O), and *VHL*-proficient cells (TK10, RXF393 and SN12C) (as gifts from Dr. Zhiyong Ding, University of Texas MD Anderson Cancer Center) were cultured in DMEM medium supplemented with 10% FBS, 100 units of *penicillin* and 100 mg/ml *streptomycin.* Mouse embryonic fibroblasts (MEFs) including *EglN1*$^{-/-}$, *EglN2*$^{-/-}$, *EglN3*$^{-/-}$, *VHL*$^{f/f}$ were described previously *(9, 31)*, and DLD1-*AKT1*$^{-/-}$*AKT2*$^{-/-}$ (termed as *AKT1/2*$^{-/-}$) was kindly provided by Dr. Bert Vogelstein (Johns Hopkins University School of Medicine), and these cells were also maintained in DMEM medium supplemented with 10% FBS. The human immortalized renal cell line HK-2 was cultured in keratinocyte serum-free medium (K-SFM, Gibco Life Technologies), supplemented with epidermal growth factor (EGF; 5 ng/ml) and bovine pituitary extract (40 pg/ml). Cell transfection was performed using Lipofectamine and Plus reagents, as described previously *(32, 33)*. Packaging of lentiviral shRNA or cDNA expressing viruses and retroviral cDNA expressing viruses, as well as subsequent infection of various cell lines were performed according to the protocols described previously *(32)*. Following viral infection, cells were maintained in the presence of hygromycin (200 μg/ml) or puromycin (1 μg/ml), depending on the viral vectors used to infect cells.

Kinase inhibitors Wortmannin (Selleck S2758), PP242 (Selleck S2218) and the proteasome inhibitor, MG132 (Enzo Life Science, BML-PI102) were used at the indicated doses. EGF (Sigma E9644), insulin (Invitrogen 41400-045) and hypoxia-mimetic agents, including Dimethyloxaloylglycine (DMOG) (Sigma D3695), Deferoxamine (DFO) (Sigma D9533) and Cobalt Chloride (C_OCl_2) (Sigma 409332) were used at the indicated doses *(34)*. Lambda Protein Phosphatase (λ-PP) (NEB P70153) was used according to the manufacturer's instructions. Hypoxia treatment was performed in a hypoxic chamber containing 1% oxygen for 16 hrs (Laboratory Products, Inc), as described previously *(6)*. PIP3 beads (P-B00Ss) were purchased from Echelon Biosciences.

Plasmid construction

Constructs of pcDNA3-HA-pVHL, pCMV-Flag-pVHL, pBabe-HA-pVHL, pLenti-Flag-EglN1, pCMV-Flag-EglN1, pCMV-Flag-EglN2, pCMV-Flag-EglN3, pCMV-Flag-HIF1α, pcDNA3-HA-HIF2α, pcDNA3-HA-HIF2α-P405A/P531A (PA) and pLenti-HIF2α-PA were described previously *(9, 31)*. pcDNA3-HA-Akt1, pcDNA3-HA-Akt2, pcDNA3-HA-Akt3 and pcDNA3-HA-myr-Akt1, pcDNA3-HA-Akt1-E17K, pGEX-GSK3β, pCMV-Flag-PDK1 were previously described (*33*). pCMV-GST-PDK1, pCMV-GST-PP2AC, pCMV-GST-pVHL, pCMV-GST-Akt1, pCMV-GST-Akt1-PH (aa1-108), pCMV-GST-Akt1-Linker (aa109-150), pCMV-GST-Akt1-KD (aa151-408), pCMV-GST-Akt1-HM (aa409-481), pCMV-GST-EglN1, pCMV-GST-EglN1-N (aa1-180) and pCMV-GST-EglN1-C (aa181-425) were cloned into mammalian expression GST-fusion vectors. pET-28-EglN1 and pET-28-EglN1-P317R were generated by sub-cloning EglN1 (WT or P317R) cDNAs into pET-28a constructs, respectively. Details of plasmid constructions are available upon request.

Various Akt1, Akt2, Akt3 and VHL mutants were generated using the QuikChange XL Site-Directed Mutagenesis Kit (Stratagene) according to the manufacturer's instructions. All mutants were generated using mutagenesis PCR and the sequences were verified by DNA sequencing. sh-Akt1-resistant mutants were generated with the specific primers as previously described *(35)*. sh-EglN1-resistant mutants were generated with the specific primers listed below:
Forward: 5'-CCTGATACGCCATTGCAATGGGAAGCTGGGCAG-3';
Reverse: 5'-CTGCCCAGCTTCCCGTTACAGTGGCGTATCAGG-3'.

shRNAs and sgRNAs

shRNA vectors to deplete endogenous *HIF1β, EglN1, EglN2, EglN3, CULLIN2, AKT1* and *HIF2α* were previously described *(16, 25, 35)*. The lentiviruses for CRISPR-Cas9 editing of *HIF2α* and *AKT3* were generated by cloning the annealed short guide RNAs (sgRNAs) into BsmBI-digested pLenti-CRISPRv2 vector, which encodes both Cas9 and an sgRNA of interest, as previously described *(36)*. The sgRNAs were designed by CRISPR Design tool (crispr.mit.edu) as listed below:
sg-Ctr Forward: 5'-CACCGCTTGTTGCGTATACGAGACT-3';
Reverse: 5'-AAACAGTCTCGTATACGCAACAAG-3';
sg-HIF2α#4 Forward: 5'-CACCGAATCTCCTCATGGTCGCA-3';
Reverse: 5'-AAACTGCGACCATGAGGAGATTC-3';
sg-HIF2α#6 Forward: 5'-CACCGTCATGAGGATGAAGTGCA-3';
Reverse: 5'-AAACTGCACTTCATCCTCATGAC-3';
sg-AKT3 Forward: 5'-CACCGAAGACAGATGGCTCATTCAT-3';
Reverse: 5'-AAACATGAATGAGCCATCTGTCTTC-3'.

Antibodies

All antibodies were used at a 1:1000 dilution in TBST buffer with 5% non-fat milk for western blot. Anti-hydroxy-HIF1α (Pro564) antibody (3434), anti-pVHL antibody (2738), anti-HIF1β antibody (5537), anti-EglN1 antibody (4835), anti-phospho-Ser473-Akt antibody (4060), anti-phospho-Thr308-Akt antibody (2965), anti-Akt1 antibody (2938), anti-Akt total antibody (4691), anti-phospho-Ser9-GSK3β antibody (5558), anti-GSK3β antibody (12456), anti-phospho-FOXO1 (Thr24)/FOXO3A (Thr32) antibody (9464), anti-FOXO3A antibody (2497), anti-GST antibody (2625), anti-pS6K1 (Thr389) antibody (9205), anti-S6K1 antibody (2708), anti-Glut1 antibody (12939) were obtained from Cell Signaling Technology. Anti-pVHL antibody (564183) was obtained from BD Biosciences. Anti-Cul2 antibody (ab166917) was obtained from Abcam. Anti-HIF1α antibody (NB100-479), anti-HIF2α antibody (NB100-122), anti-EglN2 antibody (NB100-310SS) and anti-EglN3 antibody (NB100-139SS) were obtained from Novus Biologicals. Anti-PTEN antibody (sc-7974), anti-Akt1 agarose beads (sc-5298) and polyclonal anti-HA antibody (sc-805) were obtained from Santa Cruz. Polyclonal anti-Flag antibody (F-2425), monoclonal anti-Flag antibody (F-3165, clone M2), anti-Tubulin antibody (T-5168), anti-Flag agarose beads (A-2220), anti-HA agarose beads (A-2095), peroxidase-conjugated anti-mouse secondary antibody (A-4416) and peroxidase-conjugated anti-rabbit secondary antibody (A-4914) were obtained from Sigma. Monoclonal anti-HA antibody (MMS-101P) was obtained from Covance.

The polyclonal Akt1-Pro^{125}-OH and Akt1-Pro^{313}-OH antibodies generated by Cell Signaling Technology were derived from rabbit, with each hydroxylation residue produced four clones. The antigen sequence used for immunization was Akt1 aa124-130 (S**P**SDNSG) for Pro^{125}, and Akt1 aa310-316 (CGT**P**EYL) for Pro^{313}. **P** stands for hydroxyl-proline residue in these two synthetic peptides. The antibodies were affinity purified using the antigen peptide column, but they were not counter selected on unmodified antigen.

Immunoblot (IB) and immunoprecipitation (IP) analyses

Cells were lysed in EBC buffer (50 mM Tris pH 7.5, 120 mM NaCl, 0.5% NP-40) supplemented with protease inhibitors (Complete Mini, Roche) and phosphatase inhibitors (phosphatase inhibitor cocktail set I and II, Calbiochem). The protein concentrations of whole cell lysates were measured by the Beckman Coulter DU-800 spectrophotometer using the Bio-Rad protein assay reagent as described previously *(32)*. Equal amounts of whole cell lysates were resolved by SDS-PAGE and immunoblotted with indicated antibodies. For immunoprecipitation analysis, 1000 μg lysates were incubated with the indicated antibody (1-2 μg) for 3-4 hrs at 4^{o}C followed by 1 hr incubation with Protein A/G sepharose beads (GE Healthcare). The recovered immuno-complexes were washed five times with NETN buffer (20 mM Tris, pH 8.0, 150 mM NaCl, 1 mM EDTA and 0.5% NP-40) before being resolved by SDS-PAGE and immunoblotted with indicated antibodies. Quantification of the immunoblot band intensity was performed with Image J software.

Immunohistochemistry (IHC)

Immunohistochemistry was performed on 4 micron-thick, FFPE sections using an anti-pT308-Akt monoclonal antibody (Cell Signaling Technology #2965). FFPE sections were deparaffinized using xylene and rehydrated in graded ethanol. Sections were heated with a pressure cooker to 125°C for 30 seconds and 90°C for 10 seconds in citrate buffer (pH 6.0) for antigen retrieval. All sections were incubated with peroxidase (Dako #S2003) and protein blocking reagents (Dako #X0909) for 5 minutes each. Sections were then incubated with anti-pT308-Akt (1:50) antibody diluted in Dako diluent with background reducing components (Dako #S3022) for 1 hr at room temperature. Following primary antibody incubation, sections were incubated with monoclonal mouse anti-rabbit immunoglobulins (Dako #M0737) for 30 minutes at room temperature. Afterwards, sections were incubated with Envision+ System-HRP Labeled Polymer Anti-Rabbit (Dako #K4003) for 30 minutes. All sections were developed using the DAB chromogen kit (Dako #K3468) and lightly counterstained with hematoxylin.

Validation of the anti-pT308-Akt monoclonal antibody in FFPE samples was performed using SignalSlide Phospho-Akt (Ser473) IHC Controls (Cell Signaling Technology, #8101) containing LNCaP cells with and without treatment of the phosphoinositide 3-kinase (PI3K) inhibitor, LY294002.

Purification of GST-tagged proteins

Recombinant GST-conjugated pVHL or GSK3β was generated by transforming the BL21 (DE3) *E. coli* strain with pGEX-pVHL, pGEX-GSK3β or pGEX-4T (Empty vector control). Starter cultures (5 ml) grown overnight at 37°C were inoculated (1%) into larger

volumes (500 ml). Cultures were grown at 37°C until an O.D. of 0.8, following which protein expression was induced for 12-16 hrs using 0.1 mM IPTG at 16°C with vigorous shaking. Recombinant proteins were purified from harvested pellets. Pellets were re-suspended in 5 ml EBC buffer and sonicated (5 cycles of 10 sec each at 50% output). Insoluble proteins and cell debris were discarded following centrifugation in a table-top centrifuge (13000 rpm/4°C/15 min). Each 1 ml supernatant was incubated with 50 µl of 50% Glutathione-sepharose slurry (Pierce) for 3 hrs at 4°C. The Glutathione beads were washed 3 times with EBC buffer (1 ml per wash) and stored at 4°C in EBC buffer containing 10% glycerol or eluted by elution buffer. Recovery and yield of the desired proteins (or complexes) was confirmed by analyzing 10 µl of beads by coomassie blue staining, and quantified against BSA standards.

Purification of His-tagged proteins

The recombinant wild type or mutant pVHL-Elongin B/C (VBC) complex was generated by co-transforming either wild type or mutant VHL expressing pET-pVHL (aa1-213) constructs with pACYCDuet-based Elongin B (aa1-118) and Elongin C (aa17-112) (as a gift from Dr. Yong Xiong, Yale University) by the same strategy as GST-tagged proteins. The difference was that each 1 ml supernatant was incubated with 50 µl of 50% Nickel resin slurry (Qiagen) for 3 hrs at 4°C. The Nickel resins were washed 4 times with TBS buffer (50 mM Tris pH 8.0, 120 mM NaCl) with 10 mM imidazole (Sigma) and eluted by TBS buffer with 100 mM imidazole. Recovery and yield of the desired proteins (or complexes) was confirmed by analyzing 10 µl of beads by coomassie blue staining, and quantified against BSA standards.

In vitro kinase assays

In vitro Akt kinase assays were adapted from a protocol described previously *(35)*. Briefly, 1 µg of the bacterially purified GST-GSK3β fusion proteins were incubated with immunoprecipitated Akt from different cell lysates in the presence of 200 µM ATP (with [γ-^{32}P]ATP) in the kinase reaction buffer (50 mM Tris pH 7.5, 1 mM $MnCl_2$, 2 mM DTT, 1 mM EGTA) for 30 minutes at 30^{o}C. The reaction was subsequently stopped by the addition of 3 x SDS loading buffer and resolved by SDS-PAGE. Phosphorylation of GST-GSK3β was detected by autoradiography.

Reactive Oxygen Species (ROS) assays

Cells were collected by trypsinization, re-suspended in pre-warmed phosphate-buffered saline (PBS) containing 10 µM CM-H_2DCFDA (Invitrogen), and incubated for 10 min at 37^{o}C. Mean fluorescence was determined by flow cytometry as described previously *(21)*.

In vitro PP2A dephosphorylation assays

For dephosphorylation of Akt1 by PP2A, the activated GST-fusion full-length Akt1 proteins were purified from insulin-stimulated HEK293 cells serving as the substrate, and the recombinant active PP2A was obtained from BPS Bioscience (30056). The dephosphorylation assays were performed in the PP2A phosphatase assay buffer (20 mM HEPES, pH 7.2, 100 mM NaCl and 3 mM DTT) and the reactions were incubated at 30°C for indicated time periods in the presence or absence of recombinant pVHL proteins

(Origene, TP316151). The reactions were stopped by adding 3 x SDS loading buffer and subjected to western blot analyses.

Gel filtration chromatography analyses

Cells were washed with PBS, lysed in EBC buffers containing protease inhibitors and phosphatase inhibitors, and filtered through a 0.45 μm syringe filter. Total 4 mg proteins were loaded onto a Superdex 200 10/300 GL column (GE Lifesciences Cat. No.17-5175-01). Chromatography was performed on the AKTA-FPLC (GE Lifesciences Cat. No. 18-1900-26) with EBC buffer as described previously *(37)*. One column volume of elutes was fractionated with 500 μl in each fraction, at the elution speed of 0.3 ml/min. 40 μl aliquots of each fraction were loaded onto SDS-PAGE gels and detected with indicated antibodies.

Peptide synthesis

N-terminal biotinylated peptides used for pull-down assays were synthesized at Tufts Medical School. N- and C-terminal free peptides used for *in vitro* competing assays were synthesized at LifeTein. The sequences were listed below:

Akt1-Pro^{313}-WT (aa307-328): KTFCGTPEYLAPEVLEDNDYGR;
Akt1-Pro^{313}Ala: KTFCGTAEYLAPEVLEDNDYGR;
Akt1-Pro^{318}Ala: KTFCGTPEYLAAEVLEDNDYGR;
Akt1-Pro^{313}-OH: KTFCGT**P***EYLAPEVLEDNDYGR;
Akt1-Pro^{318}-OH: KTFCGTPEYLA**P***EVLEDNDYGR;
Akt1-Pro^{125}-WT (aa115-144): EEEMDFRSGSPSDNSGAEEM;
Akt1-Pro^{125}-OH: EEEMDFRSGS**P***SDNSGAEEM;
HIF1α-WT (aa556–575): DLDLEMLAPYIPMDDDFQLR;
HIF1α-OH: DLDLEMLA**P***YIPMDDDFQLR (*denotes hydroxylation).

The FOXO3A-WT, FOXO3A-Pro^{426}-OH and FOXO3A-Pro^{426}/Pro^{437}-OH peptides were previously described (*25*). Peptides were diluted into 1 mM for further biochemical assays.

Dot immunoblot assays

Peptides were spotted onto nitrocellulose membrane allowing solution to penetrate (usually 3-4 mm diameter) by applying it slowly as a volume of 1 μl. The membrane was dried, and blocked in non-specific sites by soaking in TBST buffer with 5% non-fat milk for immunoblot analysis as described previously *(37)*.

Peptide-binding assays

Peptides (1 μg) were incubated with 1 mg of EBC extracts prepared from cells in a total volume of 500 μl for 4 hrs at 4°C and then added 10 μl Streptavidin agarose (Thermo Scientific 20353) for another 1 hr. The agarose was washed four times with NETN buffer. Bound proteins were eluted by boiling in SDS loading buffer, and resolved by SDS-PAGE, then detected with immunoblot analysis.

In vitro hydroxylation assays

In vitro hydroxylation assays were modified from a previously published *in vitro* hydroxylation assay *(25, 28)*. In brief, peptides (10 μg) or purified recombinant proteins

(1 μg) were mixed with 50 mM HEPES (pH 7.4), 1500 U/μl Catalase, 100 μM $FeSO_4$, 1 μM ascorbic acid, 0.2 μM α-ketoglutarate (α-KG), and 1 μg of purified recombinant EglN1 proteins in a 30 μl reaction volume. After incubation for 2 hrs at 37°C, the reactions were subjected to immunoblot analysis or mass spectrometry analysis.

Mass spectrometry analyses

For mass spectrometry analysis, anti-HA immunoprecipitations (IP) were performed with the whole cell lysates derived from three 10 cm dishes of HEK293 cells co-transfected with Flag-EglN1 and HA-Akt1. The IP proteins were resolved by SDS-PAGE, and identified by Coomassie staining. The band containing Akt1 was reduced with 10 mM DTT for 30 minutes, alkylated with 55 mM iodoacetamide for 45 minutes, and in-gel-digested with trypsin enzymes. The resulting peptides were extracted from the gel and analyzed by microcapillary reversed-phase (C_{18}) liquid chromatography-tandem mass spectrometry (LC-MS/MS), using a high resolution Orbitrap Elite (Thermo Fisher Scientific) in positive ion DDA mode (Top 6) via higher energy collisional dissociation (HCD) coupled to a Proxeon EASY-nLc II nano-HPLC *(38)*. MS/MS data were searched against the Uniprot Human protein database (version 20151209 containing 21,024 entries) using Mascot 2.5.1 (Matrix Science) and data analysis was performed using the Scaffold 4.4.8 software (Proteome Software). Peptides and modified peptides were accepted if they passed a 1% FDR threshold.

Colony formation assays

Cells were seeded into 6-well plates (300 or 600 cells/well) and left for 8-12 days until formation of visible colonies. Colonies were washed with PBS and fixed with 10% acetic acid/10% methanol for 20 minutes, then stained with 0.4% crystal violet in 20% ethanol for 20 minutes. After staining, the plates were washed and air-dried, and colony numbers were counted. Three independent experiments were performed to generate the standard error of the difference (SED).

Soft agar assays

The anchorage-independent cell growth assays were performed as described previously *(33)*. Briefly, the assays were preformed using 6-well plates where the solid medium consists of two layers. The bottom layer contains 0.8% noble agar and the top layer contains 0.4% agar suspended with 1 x 10^4 or 3 x10^4 cells. 500 μl complete DMEM medium was added every 7 days to keep the top layer moisture and 4 weeks later the cells were stained with iodonitrotetrazolium chloride (1 mg/ml) (sigma I10406) for colony visualization and counting. Three independent experiments were performed to generate the standard error of the difference (SED).

Mouse xenograft assays

Mouse xenograft assays were performed as described previously *(33)*. Briefly, 2 x 10^6 DLD1-*AKT1/2*$^{-/-}$ cells stably expressing EV, WT or P125/313A mutant form of Akt1 were injected into the flank of 8 female nude mice (NCRNU-M-M from Taconic, 4-5 weeks of age). Tumor size was measured every three days with a caliper, and the tumor volume was determined with the formula: L x W^2 x 0.52, where L is the longest diameter

and W is the shortest diameter. After 18 days, mice were sacrificed and xenografted solid tumors were dissected, then tumor weights were measured and recorded post-necropsy.

Statistics

Differences between control and test conditions were evaluated by Student's *t* test or one-way analysis of variance (ANOVA) test using the SPSS 11.5 Statistical Software. Values of $P < 0.05$ were considered statistically significant.

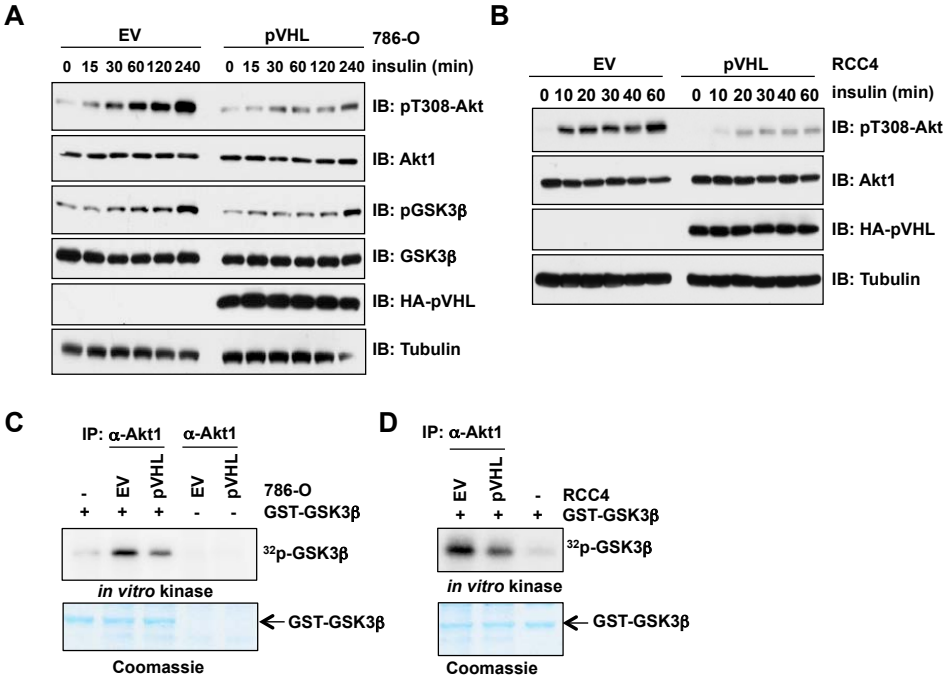

Fig. S1

pVHL suppresses Akt kinase activity. (A-B) *VHL*-deficient 786-O (A) or RCC4 (B) cells that were engineered via retroviral infection to stably express pVHL (with EV as a negative control), were serum starved for 24 hrs followed by stimulation with insulin (0.1 μM). At the indicated time points, whole cell lysates (WCL) were harvested for immunoblot (IB) analysis. (C-D) *In vitro* Akt kinase assays were performed with bacterially purified GST-GSK3β as a substrate and immunoprecipitated Akt1 from the cells in (A) and (B) as the source of kinase.

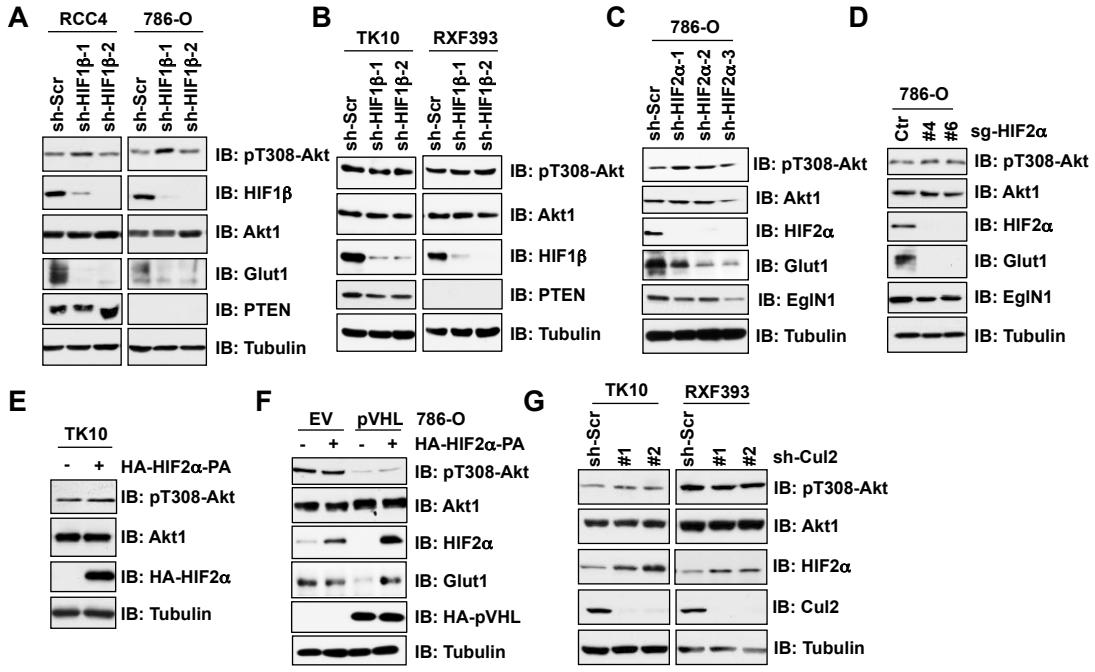

Fig. S2

Inhibition of Akt by pVHL is independent of the HIF pathway. (A-B) IB analysis of WCL derived from *VHL*-deficient (RCC4 and 786-O) (A) or *VHL*-proficient (TK10 and RXF393) (B) renal carcinoma cells lentivirally infected with sh-Scramble (sh-Scr) or multiple independent *HIF1β* shRNAs (sh-HIF1β). Infected cells were selected with puromycin (1 μg/ml) for 72 hrs before harvesting. (C) IB analysis of WCL derived from *VHL*-deficient 786-O cells lentivirally infected with sh-Scr or multiple independent *HIF2α* shRNAs (sh-HIF2α). Infected cells were selected with puromycin (1 μg/ml) for 72 hrs before harvesting. (D) IB analysis of WCL derived from *VHL*-deficient 786-O cells knocked out *HIF2α* by the CRISPR/Cas9 system with different sgRNAs (labeled with #4 and #6). (E-F) IB analysis of WCL derived from TK10 cells (E) or 786-O cells (F) engineered via retroviral infection to stably express pVHL (with EV as a negative control), which were then infected with lentivirus encoding a non-degradable HA-HIF2α mutant, in which the two characterized critical proline residues in the two oxygen-dependent degradation (ODD) motifs were mutated to alanine (termed as HIF2α-PA). (G) IB analysis of WCL derived from *VHL*-proficient TK10 and RXF393 cells that were lentivirally infected with sh-Scr or multiple independent shRNAs against *CULLIN2* (sh-Cul2).

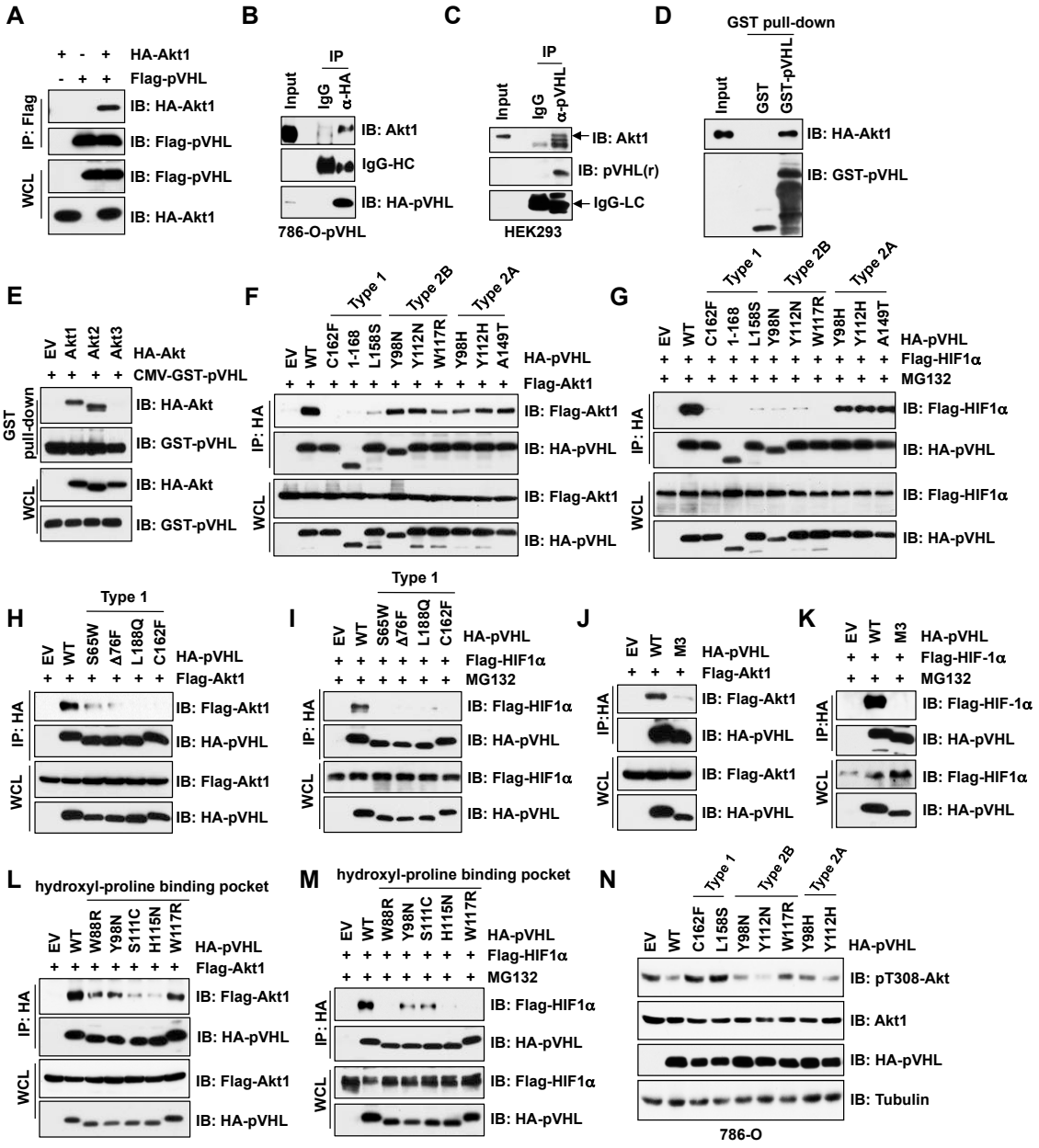
A
HA-Akt1
Flag-pVHL
IP: Flag
IB: HA-Akt1
IB: Flag-pVHL
WCL
IB: Flag-pVHL
IB: HA-Akt1
B
IP
Input
IgG
α-HA
IB: Akt1
IgG-HC
IB: HA-pVHL
786-O-pVHL
C
IP
Input
IgG
α-pVHL
IB: Akt1
IB: pVHL(r)
IgG-LC
HEK293
D
GST pull-down
Input
GST
GST-pVHL
IB: HA-Akt1
IB: GST-pVHL
E
EV
Akt1
Akt2
Akt3
HA-Akt
CMV-GST-pVHL
GST pull-down
IB: HA-Akt
IB: GST-pVHL
WCL
IB: HA-Akt
IB: GST-pVHL
F
Type 1
Type 2B
Type 2A
EV
WT
C162F
1-168
L158S
Y98N
Y112N
W117R
Y98H
Y112H
A149T
HA-pVHL
Flag-Akt1
IP: HA
IB: Flag-Akt1
IB: HA-pVHL
WCL
IB: Flag-Akt1
IB: HA-pVHL
G
Type 1
Type 2B
Type 2A
EV
WT
C162F
1-168
L158S
Y98N
Y112N
W117R
Y98H
Y112H
A149T
HA-pVHL
Flag-HIF1α
MG132
IP: HA
IB: Flag-HIF1α
IB: HA-pVHL
WCL
IB: Flag-HIF1α
IB: HA-pVHL
H
Type 1
EV
WT
S65W
Δ76F
L188Q
C162F
HA-pVHL
Flag-Akt1
IP: HA
IB: Flag-Akt1
IB: HA-pVHL
WCL
IB: Flag-Akt1
IB: HA-pVHL
I
Type 1
EV
WT
S65W
Δ76F
L188Q
C162F
HA-pVHL
Flag-HIF1α
MG132
IP: HA
IB: Flag-HIF1α
IB: HA-pVHL
WCL
IB: Flag-HIF1α
IB: HA-pVHL
J
EV
WT
M3
HA-pVHL
Flag-Akt1
IP:HA
IB: Flag-Akt1
IB: HA-pVHL
WCL
IB: Flag-Akt1
IB: HA-pVHL
K
EV
WT
M3
HA-pVHL
Flag-HIF-1α
MG132
IP:HA
IB: Flag-HIF-1α
IB: HA-pVHL
WCL
IB: Flag-HIF1α
IB: HA-pVHL
L
hydroxyl-proline binding pocket
EV
WT
W88R
Y98N
S111C
H115N
W117R
HA-pVHL
Flag-Akt1
IP: HA
IB: Flag-Akt1
IB: HA-pVHL
WCL
IB: Flag-Akt1
IB: HA-pVHL
M
hydroxyl-proline binding pocket
EV
WT
W88R
Y98N
S111C
H115N
W117R
HA-pVHL
Flag-HIF1α
MG132
IP: HA
IB: Flag-HIF1α
IB: HA-pVHL
WCL
IB: Flag-HIF1α
IB: HA-pVHL
N
Type 1
Type 2B
Type 2A
EV
WT
C162F
L158S
Y98N
Y112N
W117R
Y98H
Y112H
HA-pVHL
IB: pT308-Akt
IB: Akt1
IB: HA-pVHL
IB: Tubulin
786-O

Fig. S3

VHL disease-associated mutations affect the interaction between pVHL and Akt. (A) IB analysis of IP and WCL derived from HEK293 cells transfected with the indicated constructs. (B) IB analysis of anti-HA IP and WCL derived from 786-O-pVHL cells that ectopically expressed HA-tagged pVHL. IgG was used as a negative control. IgG-HC, IgG heavy chain. (C) IP analysis to detect the interaction between endogenous pVHL and endogenous Akt1 in HEK293 cells. IgG was used as a negative control. IgG-LC, IgG light chain. (D) GST pull-down analysis to show that bacterially purified recombinant GST-pVHL interacts with Akt1 derived from HEK293 cells. Recombinant GST protein was used as a negative control. (E) GST pull-down analysis to show that GST-pVHL purified from mammalian cells specifically interacts with Akt1 and Akt2, but not Akt3 that were ectopically expressed in HEK293 cells. (F-M) IB analysis of anti-HA IP and WCL derived from 293T cells co-transfected with Flag-HIF1α or Flag-Akt1 and various mutants of HA-pVHL constructs. 30 hrs post-transfection, cells transfected with HIF1α were treated with 10 μM MG132 for 12 hrs before harvesting. M3 indicated a pVHL mutant harboring triple mutations (S111G/H115L/W117G). (N) IB analysis of WCL derived from *VHL*-deficient 786-O cells retrovirally infected with different VHL mutants. Infected cells were selected with puromycin (1 μg/ml) for 72 hrs before harvesting.

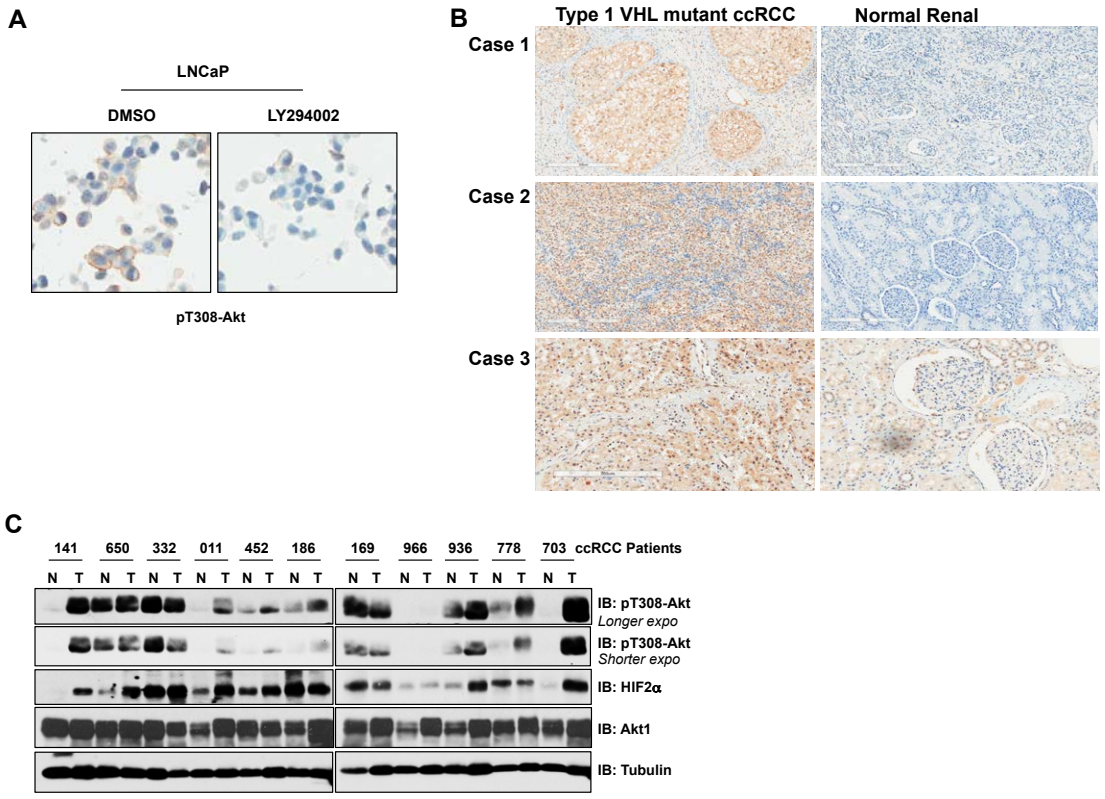

Fig. S4

pT308-Akt signal increases in *VHL* mutant ccRCC. (A) Validation of the anti-pT308-Akt monoclonal antibody in FFPE samples was performed using LNCaP cells with or without treatment of the PI3K inhibitor, LY294002. (B) Immunohistochemistry (IHC) staining of pT308-Akt in matched type 1 VHL mutant ccRCC and normal renal cortex. A relatively high degree of positive membranous, cytoplasmic, and nuclear staining has been observed in tumor specimens (left panel). In contrast, minimal cytoplasmic staining has been observed in the corresponding renal cortexes (right panel) of these cases. (C) IB analysis to detect a positive correlation between Akt phosphorylation and HIF2α accumulation in WCL derived from human ccRCC samples. N, indicated adjacent normal tissue, and T, indicated ccRCC samples.

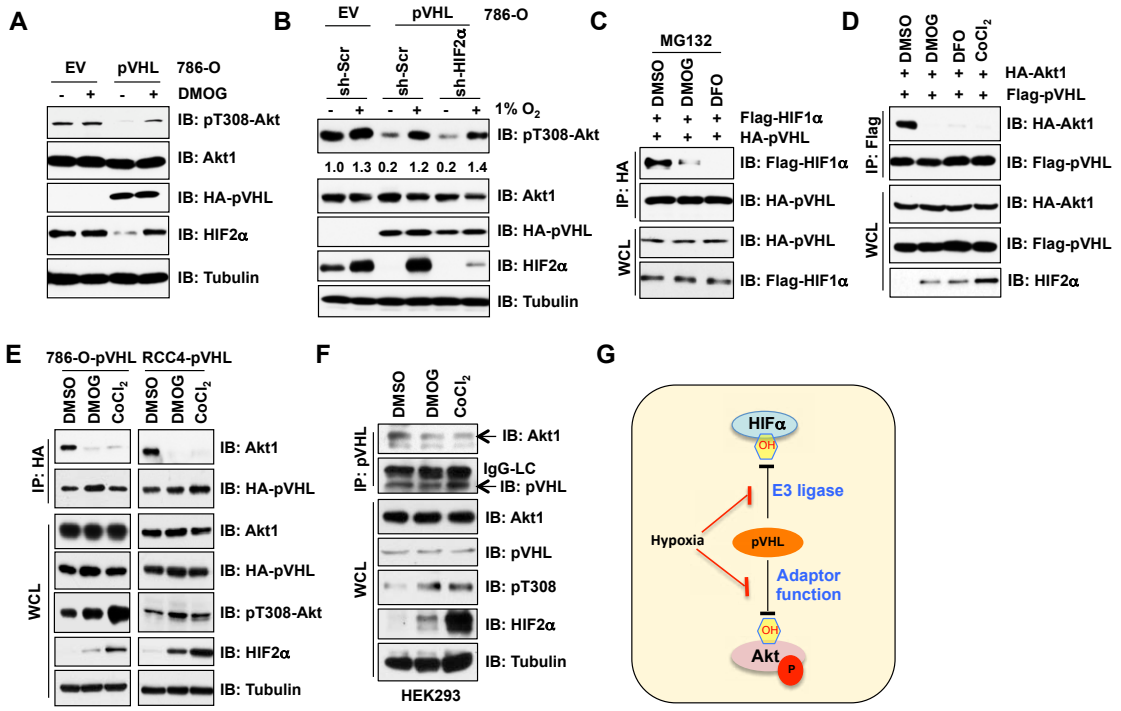

Fig. S5

pVHL interacts with Akt1 in a proline-hydroxylation dependent manner. (A) IB analysis of WCL derived from *VHL*-deficient 786-O cells infected with the indicated retroviruses. Infected cells were selected with puromycin (1 μg/ml) for 72 hrs and treated with DMOG (200 μM) or DMSO for 16 hrs before harvesting. (B) 786-O-pVHL cells lentivirally infected with sh-Scr or shRNAs against *HIF2α* (sh-HIF2α) were cultured in 1% O_2 or normal conditions before harvesting for IB analysis. The relative Akt phosphorylation (pT308) status were quantified upon normalization for total Akt1 expressed as fold induction over control, and listed at each lane below. (C-D) IB analysis of IP and WCL derived from HEK293 cells co-transfected pVHL with HIF1α (C) or Akt1 (D). Cells were treated with hypoxia mimetic reagents DMOG (200 μM), DFO (200 μM) or $CoCl_2$ (200 μM) (with DMSO as a negative control) for 4 hrs before harvesting for IB analysis. In (C), cells were treated with MG132 (10 μM) 12 hrs before harvesting. (E) IB analysis of IP and WCL derived from *VHL*-deficient RCC and 786-O cells that were engineered to stably express HA-pVHL. Resulting cells were treated with hypoxia mimetic reagents DMOG (200 μM), or $CoCl_2$ (200 μM) for 4 hrs before harvesting. DMSO was used as a negative control. (F) pVHL antibody immunoprecipitations and WCL derived from HEK293 cells treated with hypoxia mimetic reagents to detect changes in interaction of endogenous Akt1 and pVHL. IgG-LC, indicated IgG light chain. (G) A schematic illustration of how the interaction of pVHL with HIFα or Akt can be disrupted by hypoxia, respectively.

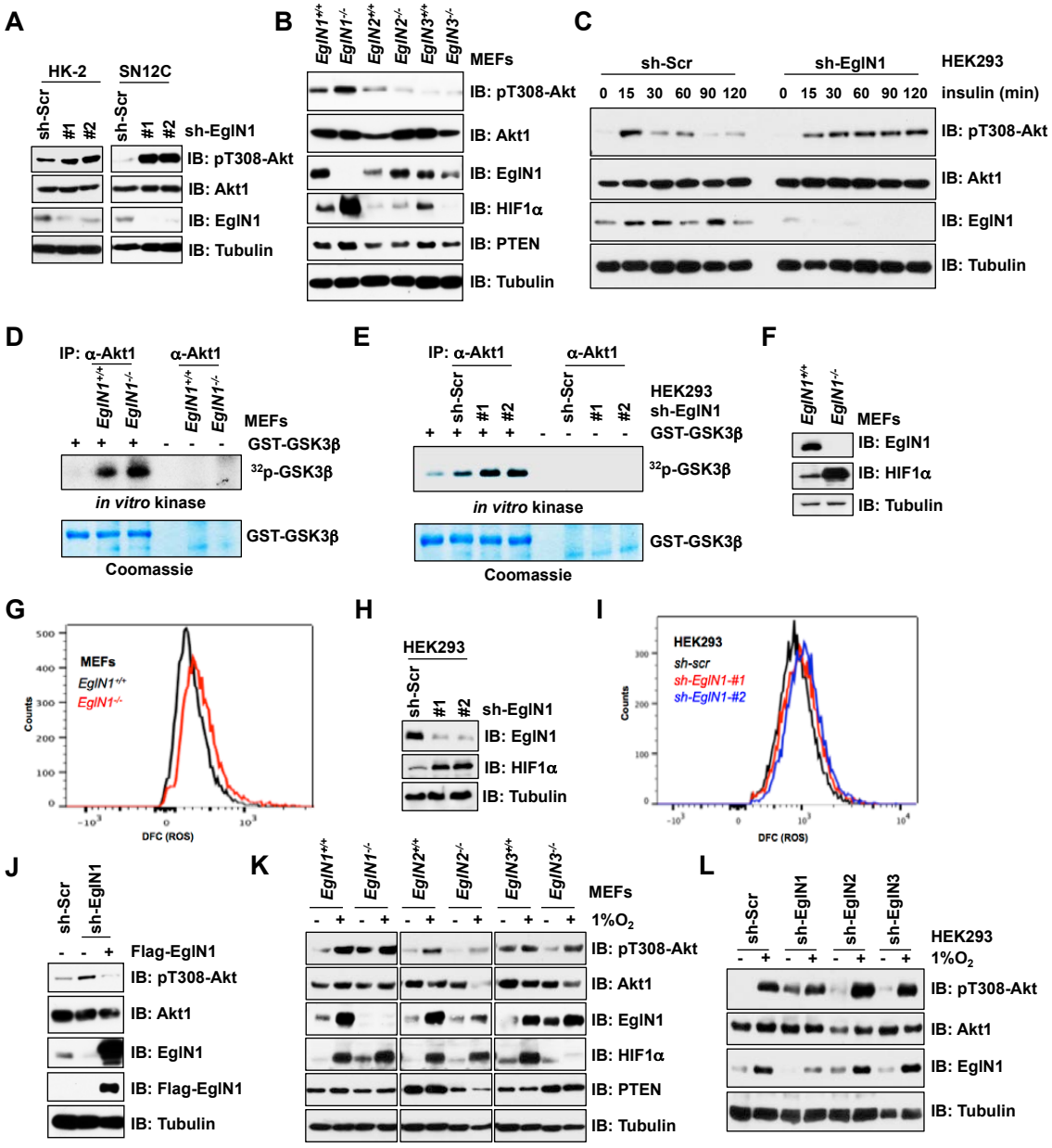
A
HK-2
SN12C
sh-Scr
#1
#2
sh-EglN1
IB: pT308-Akt
IB: Akt1
IB: EglN1
IB: Tubulin
B
EglN1+/+
EglN1-/-
EglN2+/+
EglN2-/-
EglN3+/+
EglN3-/-
MEFs
IB: pT308-Akt
IB: Akt1
IB: EglN1
IB: HIF1α
IB: PTEN
IB: Tubulin
C
sh-Scr
sh-EglN1
HEK293
0 15 30 60 90 120
0 15 30 60 90 120
insulin (min)
IB: pT308-Akt
IB: Akt1
IB: EglN1
IB: Tubulin
D
IP: α-Akt1
α-Akt1
EglN1+/+
EglN1-/-
MEFs
GST-GSK3β
32p-GSK3β
in vitro kinase
GST-GSK3β
Coomassie
E
IP: α-Akt1
α-Akt1
sh-Scr
#1
#2
HEK293
sh-EglN1
GST-GSK3β
32p-GSK3β
in vitro kinase
GST-GSK3β
Coomassie
F
EglN1+/+
EglN1-/-
MEFs
IB: EglN1
IB: HIF1α
IB: Tubulin
G
MEFs
EglN1+/+
EglN1-/-
Counts
DFC (ROS)
H
HEK293
sh-Scr
#1
#2
sh-EglN1
IB: EglN1
IB: HIF1α
IB: Tubulin
I
HEK293
sh-scr
sh-EglN1-#1
sh-EglN1-#2
Counts
DFC (ROS)
J
sh-Scr
sh-EglN1
Flag-EglN1
IB: pT308-Akt
IB: Akt1
IB: EglN1
IB: Flag-EglN1
IB: Tubulin
K
EglN1+/+
EglN1-/-
EglN2+/+
EglN2-/-
EglN3+/+
EglN3-/-
MEFs
1%O2
IB: pT308-Akt
IB: Akt1
IB: EglN1
IB: HIF1α
IB: PTEN
IB: Tubulin
L
sh-Scr
sh-EglN1
sh-EglN2
sh-EglN3
HEK293
1%O2
IB: pT308-Akt
IB: Akt1
IB: EglN1
IB: Tubulin

Fig. S6

EglN1 inhibits Akt kinase activity. (A) *VHL*-proficient renal epithelia cell line HK-2 and renal carcinoma cell line SN12C were lentivirally infected with sh-Scr or multiple independent *EglN1* shRNAs (sh-EglN1). Infected cells were selected with puromycin (1 μg/ml) for 72 hrs before harvesting for IB analysis. (B) IB analysis of WCL derived from *EglN1*$^{-/-}$, *EglN2*$^{-/-}$, *EglN3*$^{-/-}$ or wild type counterpart MEFs. (C) HEK293 cells lentivirally infected with the indicated shRNAs, were serum starved for 24 hrs followed by stimulation with insulin (0.1 μM). At the indicated time points, WCL were harvested for IB analysis. (D-E) Akt *in vitro* kinase assays were performed with bacterially purified GST-GSK3β as a substrate and immunoprecipitated Akt1 from the cells deleted *EglN1* as the source of kinase. (F-I) *EglN* knockdown or knockout cells were used to detect cellular ROS levels by flow cytometer analyses (G and I). Genetic ablation of *EglN1* in MEFs or knockdown efficiency of *EglN1* in HEK293 cells was confirmed in (F and H), respectively. (J) HEK293 cells were infected with sh-Scr or sh-EglN1 lentivirus to deplete endogenous *EglN1*. Resulting cells were lentivirally re-introduced with EV or engineered sh-resistant EglN1 cDNA. Infected cells were selected with puromycin (1 μg/ml) for 72 hrs before harvesting for IB analysis. (K and L) IB analysis of WCL from *EglN* deleted cells with or without exposure to 1% O_2 for 16 hrs before harvesting.

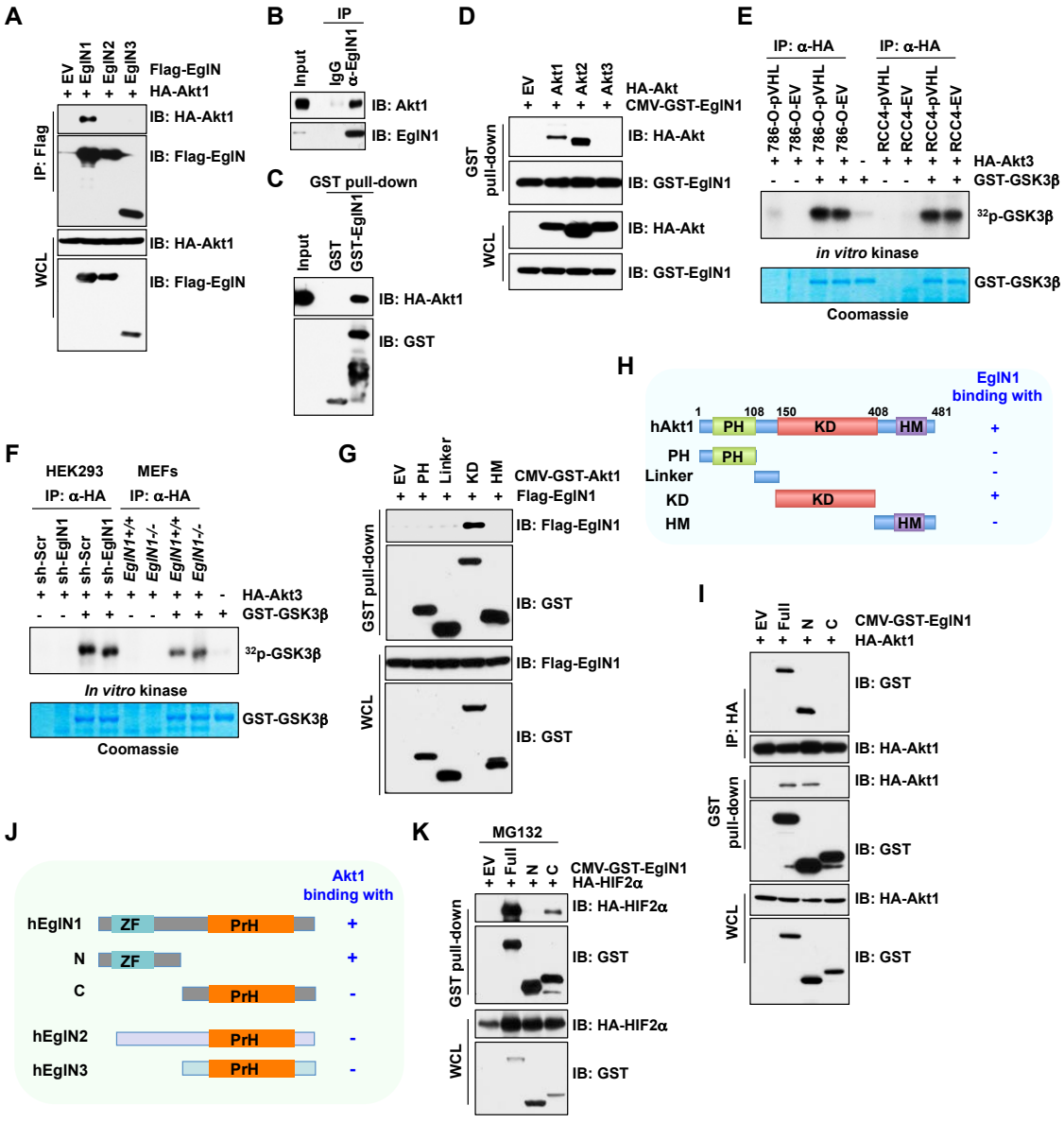
A
EV
EglN1
EglN2
EglN3
Flag-EglN
HA-Akt1
IP: Flag
IB: HA-Akt1
IB: Flag-EglN
WCL
IB: HA-Akt1
IB: Flag-EglN
B
IP
Input
IgG
α-EglN1
IB: Akt1
IB: EglN1
C
GST pull-down
Input
GST
GST-EglN1
IB: HA-Akt1
IB: GST
D
EV
Akt1
Akt2
Akt3
HA-Akt
CMV-GST-EglN1
GST pull-down
IB: HA-Akt
IB: GST-EglN1
WCL
IB: HA-Akt
IB: GST-EglN1
E
IP: α-HA
IP: α-HA
786-O-pVHL
786-O-EV
RCC4-pVHL
RCC4-EV
HA-Akt3
GST-GSK3β
32p-GSK3β
in vitro kinase
GST-GSK3β
Coomassie
F
HEK293
MEFs
IP: α-HA
IP: α-HA
sh-Scr
sh-EglN1
EglN1+/+
EglN1-/-
HA-Akt3
GST-GSK3β
32p-GSK3β
In vitro kinase
GST-GSK3β
Coomassie
G
EV
PH
Linker
KD
HM
CMV-GST-Akt1
Flag-EglN1
GST pull-down
IB: Flag-EglN1
IB: GST
WCL
IB: Flag-EglN1
IB: GST
H
EglN1 binding with
hAkt1
PH
KD
HM
1
108
150
408
481
+
PH
-
Linker
-
KD
+
HM
-
I
EV
Full
N
C
CMV-GST-EglN1
HA-Akt1
IP: HA
IB: GST
IB: HA-Akt1
GST pull-down
IB: HA-Akt1
IB: GST
WCL
IB: HA-Akt1
IB: GST
J
Akt1 binding with
hEglN1
ZF
PrH
+
N
ZF
+
C
PrH
-
hEglN2
PrH
-
hEglN3
PrH
-
K
MG132
EV
Full
N
C
CMV-GST-EglN1
HA-HIF2α
GST pull-down
IB: HA-HIF2α
IB: GST
WCL
IB: HA-HIF2α
IB: GST

Fig. S7

EglN1 interacts with Akt largely through the N-terminal zinc finger (ZF) domain. (A-D) Co-immunoprecipitations (co-IP) and GST pull-down assays to show that Akt1 specifically interacts with EglN1 (A), and EglN1 interacts with Akt1 and Akt2, but not with Akt3 (B-D) in HEK293 cells at endogenous levels or at ectopic expression conditions. (E-F) Akt3 *in vitro* kinase assays were performed with bacterially purified GST-GSK3β as a substrate and immuno-purified ectopically expressing HA-Akt3 from *VHL*-deficient 786-O and RCC4 cells (E), or *EglN1*$^{-/-}$ MEFs and *EglN1*-depleted HEK293 cells (F) as the source of kinase. (G-H) GST pull-down assays to show that ectopically expressing Akt1 fragments (H) specifically interacted with Flag-EglN1 in 293T cells (G). PH, Pleckstrin homology domain; KD, kinase domain; HM, hydrophobic motif. (I) GST pull-down assays were performed with WCL derived from HEK293 cells transfected with HA-Akt1 and various fragments of CMV-GST-EglN1 constructs to illustrate that EglN1 interacts with Akt1 largely through the N-terminal ZF domain. (J) A schematic illustration of the functional domains in various EglN isoforms as well as the unique N-terminal ZF domain in EglN1 that mediates the specific interaction between Akt1 and EglN1, but not EglN2 or EglN3. N, N-terminal of EglN1 with zinc finger (ZF) domain; C, C-terminal of EglN1 with prolyl hydroxylase (PrH) domain. (K) GST pull-down assays to illustrate that unlike Akt1, HIF2α mainly interacted with the C-terminal of EglN1.

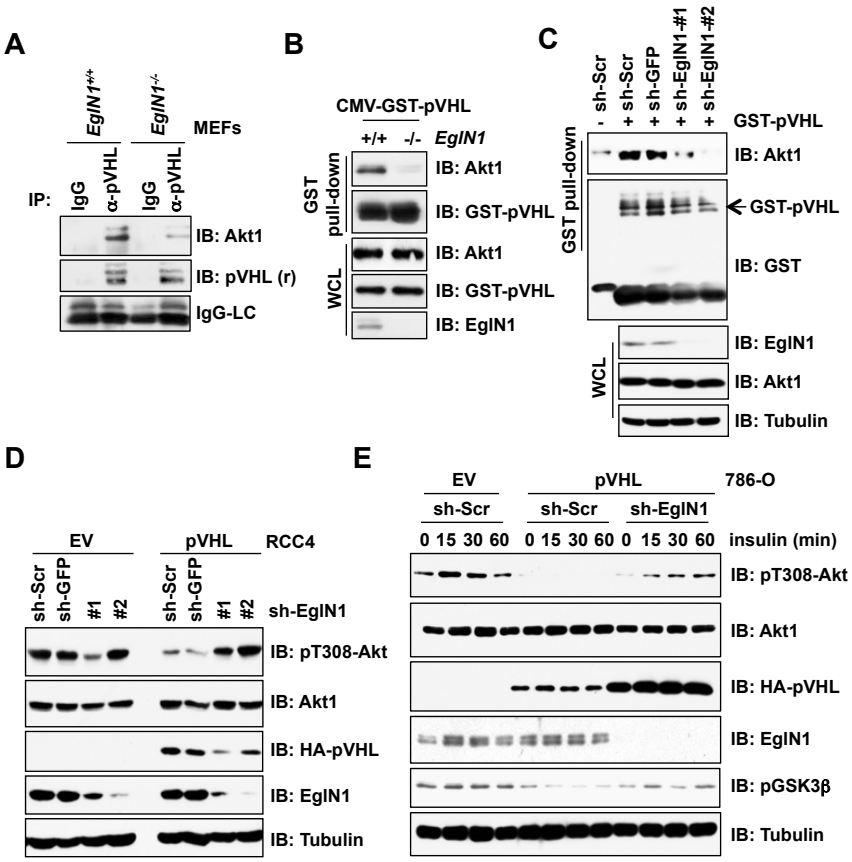

Fig. S8

Depletion of endogenous *EglN1* impairs the interaction of pVHL with Akt in cells. (A) IB analysis of immunoprecipitations of endogenous pVHL with WCL derived from *EglN1*$^{-/-}$ or WT counterpart MEFs. IgG was used as a negative control. IgG-LC, indicated IgG light chain. (B) GST pull-down analysis with WCL derived from *EglN1*$^{-/-}$ or WT counterpart MEFs transfected with GST tagged pVHL. (C) GST pull-down assays were performed with bacterially purified recombinant GST-pVHL and WCL derived from HEK293 cells lentivirally infected with the indicated shRNAs to illustrate that depleting endogenous *EglN1* largely abolished the interaction between pVHL and endogenous Akt1. Infected cells were selected with puromycin (1 μg/ml) for 72 hrs before the pull-down assays, where GST was used as a negative control. (D) RCC4 cells infected with EV or pVHL retrovirus to generate cells stably expressing HA-pVHL. Resulting cells were lentivirally infected with sh-Scr or shRNAs against *EglN1* (sh-EglN1) to deplete endogenous *EglN1*. Infected cells were selected with puromycin (1 μg/ml) for 72 hrs before harvesting for IB analysis. (E) 786-O cells infected with control (EV) or pVHL retrovirus to generate cells stably expressing HA-pVHL. Resulting cells were infected with sh-Scr or sh-EglN1 lentivirus. Resulting cells were serum starved for 24 hrs followed by stimulation with insulin (0.1 μM). At the indicated time points, WCL were harvested for IB analysis.

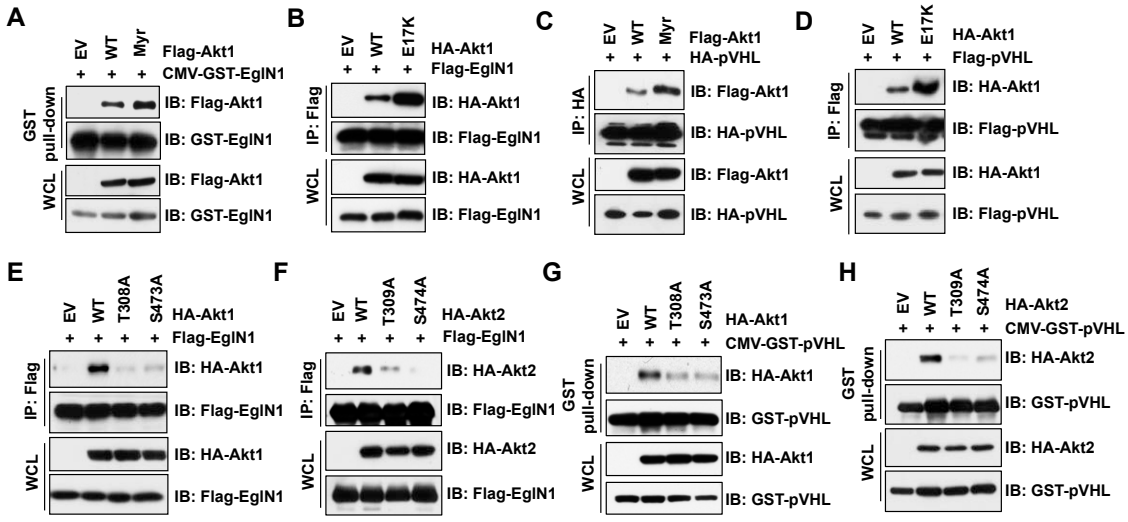

Fig. S9

EglN1 and pVHL preferentially interact with the activated form of Akt. (A) GST pull-down analysis of WCL derived from HEK293 cells transfected with the indicated constructs. (B-F) IB analysis of co-immunoprecipitations (co-IP) and WCL derived from HEK293 cells transfected with the indicated constructs. (G-H) GST pull-down analysis of WCL derived from HEK293 cells transfected with the indicated constructs.

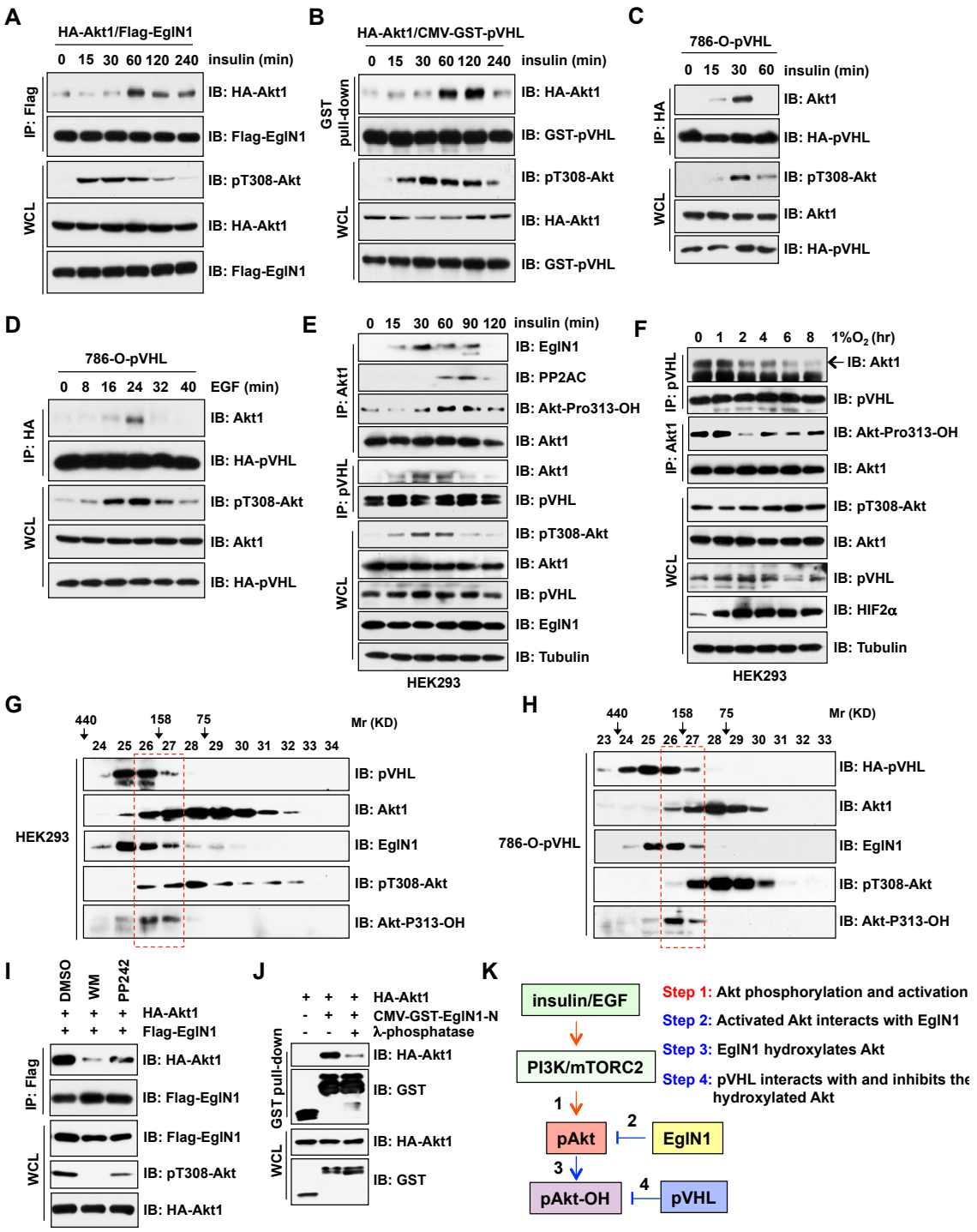
A
HA-Akt1/Flag-EglN1
0 15 30 60 120 240 insulin (min)
IP: Flag
IB: HA-Akt1
IB: Flag-EglN1
WCL
IB: pT308-Akt
IB: HA-Akt1
IB: Flag-EglN1
B
HA-Akt1/CMV-GST-pVHL
0 15 30 60 120 240 insulin (min)
GST pull-down
IB: HA-Akt1
IB: GST-pVHL
WCL
IB: pT308-Akt
IB: HA-Akt1
IB: GST-pVHL
C
786-O-pVHL
0 15 30 60 insulin (min)
IP: HA
IB: Akt1
IB: HA-pVHL
WCL
IB: pT308-Akt
IB: Akt1
IB: HA-pVHL
D
786-O-pVHL
0 8 16 24 32 40 EGF (min)
IP: HA
IB: Akt1
IB: HA-pVHL
WCL
IB: pT308-Akt
IB: Akt1
IB: HA-pVHL
E
0 15 30 60 90 120 insulin (min)
IP: Akt1
IB: EglN1
IB: PP2AC
IB: Akt-Pro313-OH
IP: pVHL
IB: Akt1
IB: Akt1
IB: pVHL
WCL
IB: pT308-Akt
IB: Akt1
IB: pVHL
IB: EglN1
IB: Tubulin
HEK293
F
0 1 2 4 6 8 1%O2 (hr)
IP: pVHL
IB: Akt1
IB: pVHL
IP: Akt1
IB: Akt-Pro313-OH
IB: Akt1
WCL
IB: pT308-Akt
IB: Akt1
IB: pVHL
IB: HIF2α
IB: Tubulin
HEK293
G
440 158 75 Mr (KD)
24 25 26 27 28 29 30 31 32 33 34
HEK293
IB: pVHL
IB: Akt1
IB: EglN1
IB: pT308-Akt
IB: Akt-P313-OH
H
440 158 75 Mr (KD)
23 24 25 26 27 28 29 30 31 32 33
786-O-pVHL
IB: HA-pVHL
IB: Akt1
IB: EglN1
IB: pT308-Akt
IB: Akt-P313-OH
I
DMSO
WM
PP242
+ + + HA-Akt1
+ + + Flag-EglN1
IP: Flag
IB: HA-Akt1
IB: Flag-EglN1
WCL
IB: Flag-EglN1
IB: pT308-Akt
IB: HA-Akt1
J
+ + + HA-Akt1
- + + CMV-GST-EglN1-N
- - + λ-phosphatase
GST pull-down
IB: HA-Akt1
IB: GST
WCL
IB: HA-Akt1
IB: GST
K
insulin/EGF
PI3K/mTORC2
1
pAkt
2
EglN1
3
pAkt-OH
4
pVHL
Step 1: Akt phosphorylation and activation
Step 2: Activated Akt interacts with EglN1
Step 3: EglN1 hydroxylates Akt
Step 4: pVHL interacts with and inhibits the hydroxylated Akt

Fig. S10

The interaction of Akt1 with EglN1 or pVHL fluctuates after the stimulation with insulin or epidermal growth factor (EGF), which largely correlates with the status of pT308-Akt in cells. (A-B) IB analysis of co-IP and WCL derived from HEK293 cells co-transfected with HA-Akt1 and Flag-EglN1 (A) or CMV-GST-pVHL (B). Resulting cells were serum starved for 24 hrs followed by stimulation with insulin (0.1 μM). At the indicated time points, WCL were harvested for IB analysis. (C-D) IB analysis of co-IP and WCL derived from *VHL*-deficient 786-O cells that were retrovirally infected to stably express HA-pVHL. Resulting cells were serum starved for 48 hrs followed by stimulation with insulin (0.1 μM) (C) or EGF (100 ng/ml) (D). At the indicated time points, WCL were harvested for co-IP and further for IB analysis. (E-F) IB analysis of co-IP and WCL derived from HEK293 cells that were serum starved for 24 hrs followed by stimulation with insulin (0.1 μM) (E) or in serum supplemented condition exposed to 1% O_2 (F). At the indicated time points, WCL were harvested for co-IP with indicated antibodies, which were further subjected to IB analysis. (G-H) IB analysis of the Gel-filtration fractions with WCL derived from HEK293 (G) or 786-O-pVHL (H) cells. (I) IB analysis of co-IP and WCL derived from HEK293 cells transfected with the indicated constructs. Where indicated, cells were treated with Wortmannin (WM) (0.2 μM) or PP242 (1 μM) for 1 hr before harvesting for IB analysis. (J) GST pull-down assays were performed with GST-EglN1-N purified from 293T cells that was incubated with WCL derived from HEK293 cells transfected with HA-Akt1. Where indicated, WCL were treated with λ-phosphatase for 30 minutes at 37^{o}C before performing GST pull-down assays. GST was used as a negative control. (K) A proposed model to illustrate a possible role of EglN1 and pVHL in contributing to the oscillation of Akt activity upon the growth factor stimulation. Specifically, the activated Akt triggered by insulin/EGF was recognized and hydroxylated by the prolyl hydroxylase EglN1. Subsequently, the proline-hydroxylated species of Akt were inhibited in part by the recruitment of tumor suppressor pVHL.

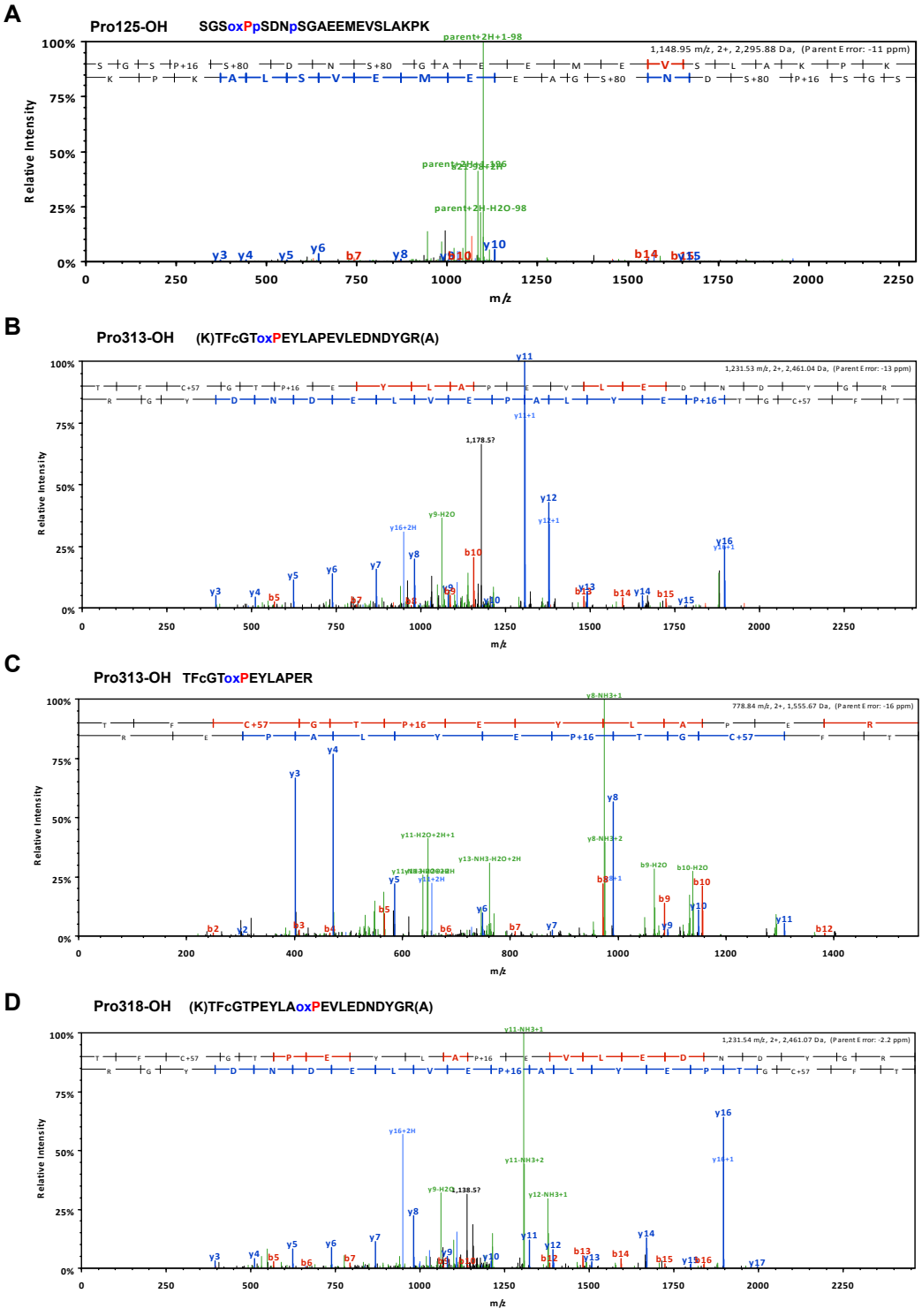
A
Pro125-OH SGSoxPpSDNpSGAEEMEVSLAKPK
B
Pro313-OH (K)TFcGToxPEYLAPEVLEDNDYGR(A)
C
Pro313-OH TFcGToxPEYLAPER
D
Pro318-OH (K)TFcGTPEYLAoxPEVLEDNDYGR(A)
Relative Intensity
m/z

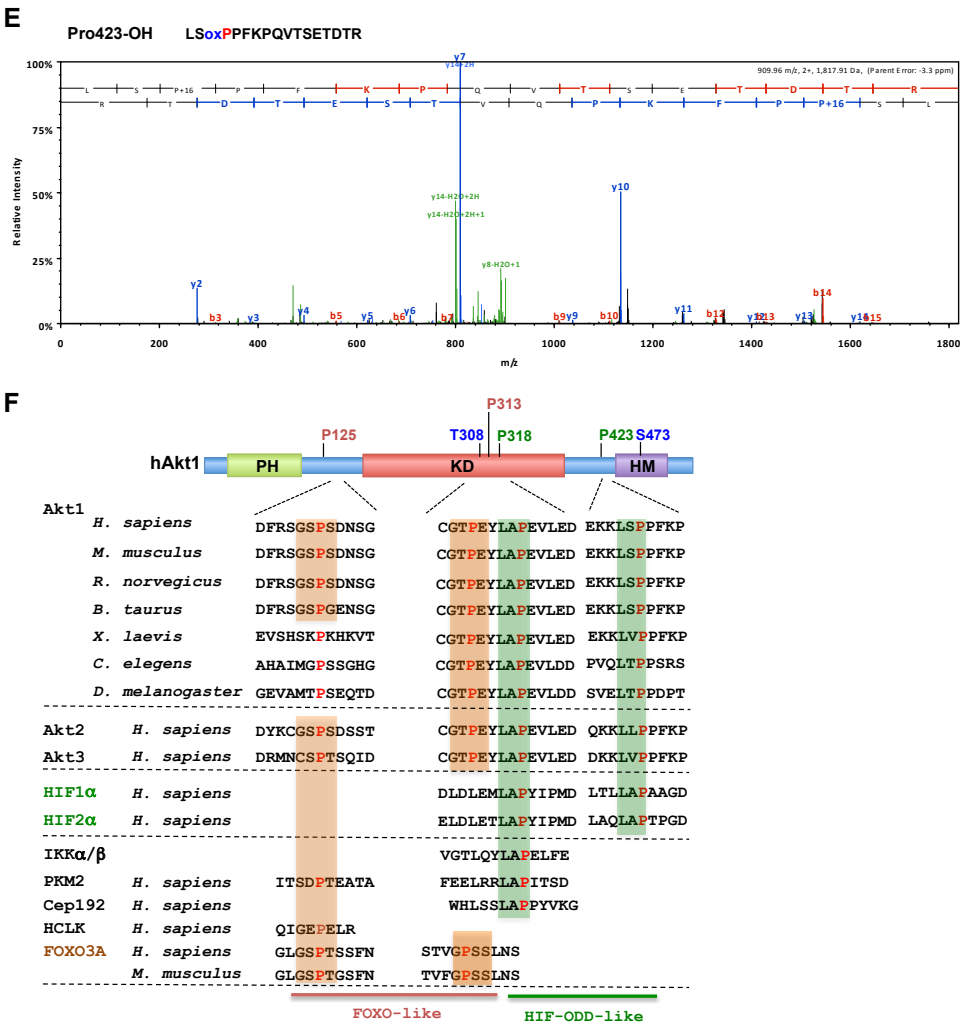

Fig. S11

Identification of Akt1 proline-hydroxylation sites by high-resolution tandem mass spectrometry analyses. (A-E) Representative LC-MS/MS spectra showing hydroxyl-proline-containing fragments derived from Akt1 immunoprecipitation of WCL derived from HEK293 cells co-transfected with HA-Akt1 and Flag-EglN1. The shift in the y- series ions after **y17** (A), **y15** (B), **y7** (C), **y10** (D) and **y13** (E) shows that the remaining peptide fragments contain a proline hydroxylation event since the detected molecular weight was shifted by exactly 15.99 Da. Notably, the spectrum is dominated by y- series ions generated from the C-terminus rather than b- series ions. To further confirm the detected Pro^{313}-hydroxylation event, we introduced a V320R mutation into Akt1 to form a new trypsin digest site to generate a shorter peptide after trypsin digestion for subsequent MS analysis, which also detected the Pro^{313} hydroxylation event (C). (F) A schematic illustration of the domain structures and various identified proline-hydroxylation sites in Akt1, as well as the sequence alignment with different Akt isoforms among species to illustrate that these proline sites are evolutionarily conserved. FOXO-like and HIF-ODD-like motifs were labeled in red and green, respectively.

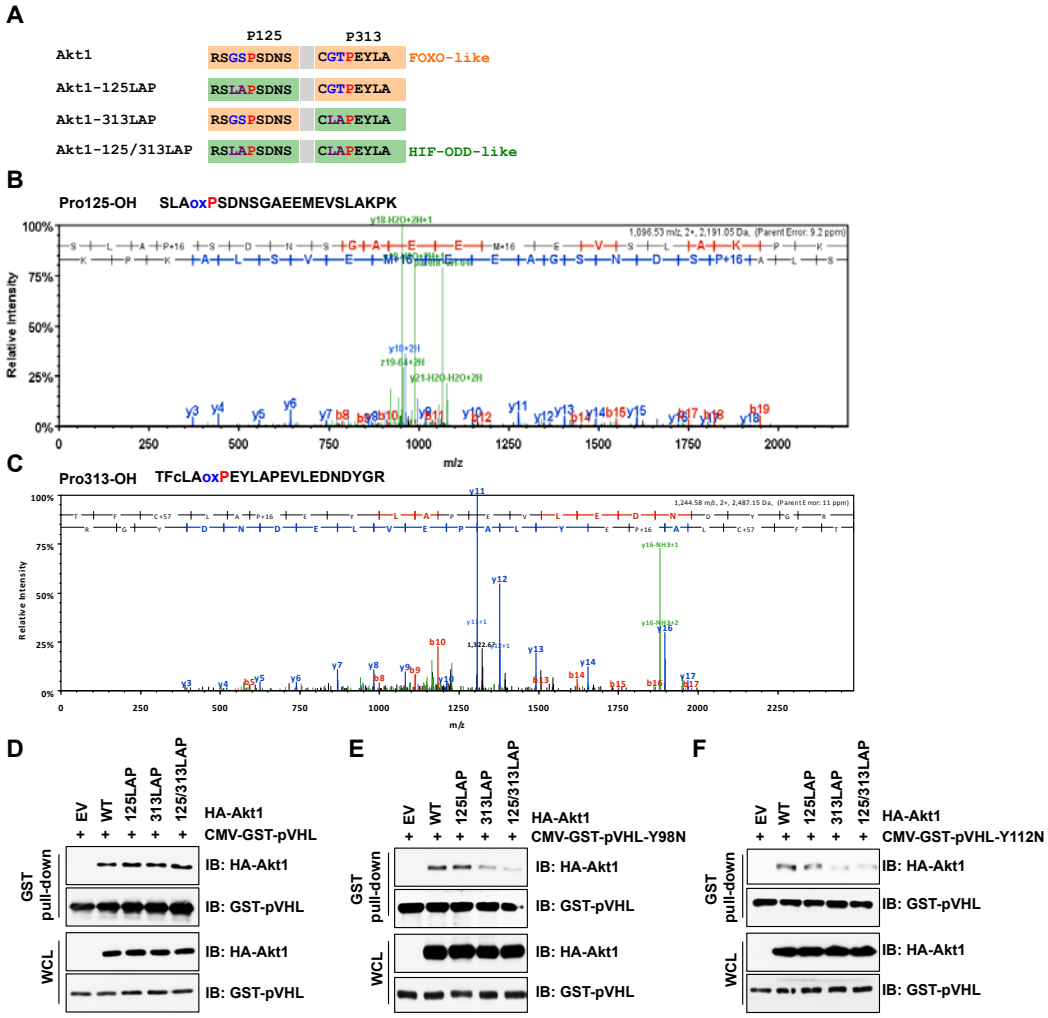

Fig. S12

Exchanging the FOXO-like motifs in Akt1 to HIF-ODD-like motifs impairs the ability of the resulting Akt mutant to interact with indicated type 2 VHL mutants. (A) Akt1 FOXO-like hydroxylation motifs were exchanged individually or in combination to HIF-ODD-like motifs (from GSP or GTP to LAP) to generate a HIF-like Akt1 mutant. (B-C) LC-MS/MS analyses were performed with immune-precipitated HA-Akt1 derived from HEK293 cells co-transfected with the HA-Akt1-125/313LAP mutant and Flag-EglN1. The shift in the y- series ions after **y17** (B) and **y15** (C) shows that the remaining peptide fragments contain a proline hydroxylation event since the detected molecular weight was shifted by exactly 15.99 Da. Notably, the spectrum is dominated by y- series ions generated from the C-terminus rather than b- series ions. (D-F) IB analysis of the GST pull-down or WCL derived from HEK293 cells co-transfected wild-type or mutant forms of Akt1 with either wild-type or indicated type 2 mutant forms of pVHL.

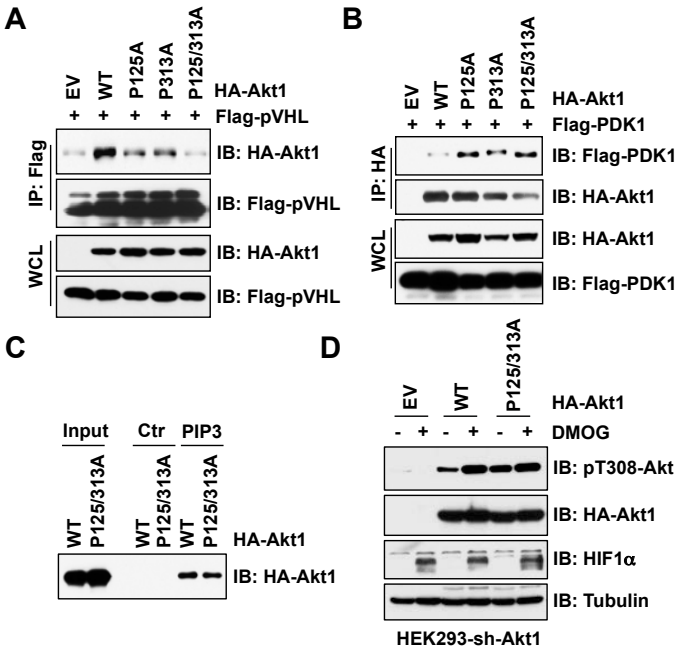

Fig. S13

Mutating Akt proline-hydroxylation sites enhances the interaction of Akt with its upstream activating kinase, PDK1. (A-B) IB analysis of co-IP and WCL derived from HEK293 cells transfected with indicated constructs. (C) Phosphatidylinositol (3,4,5)-trisphosphate (PIP3) binding assays were performed with PIP3 polysome containing beads incubated with WCL derived from HEK293 cells transfected with WT or P125/313A mutant form of Akt1 to show that mutating these two critical proline residues did not affect the ability of Akt-PH domain to interact with PIP3. Where indicated, control beads were used as a negative control. (D) HEK293 cells were lentivirally infected with sh-Akt1 to delete endogenous Akt1, and resulting cells were re-introduced WT or P125/P313A mutant form of Akt1 by retroviral infection. After treating DMOG (200 μM) for 16 hrs, cells were harvested for IB analysis.

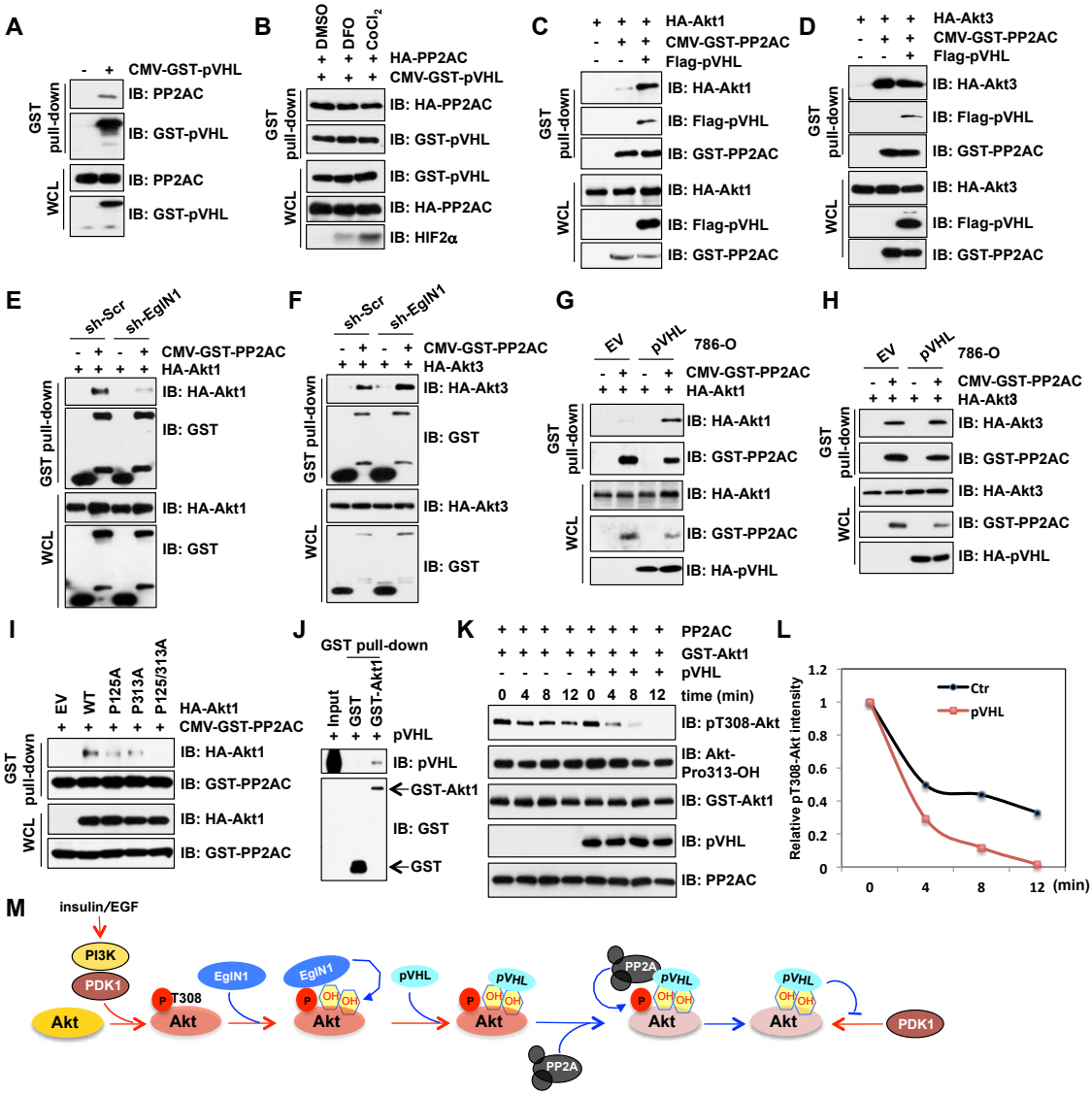
A
CMV-GST-pVHL
GST pull-down
IB: PP2AC
IB: GST-pVHL
WCL
IB: PP2AC
IB: GST-pVHL
B
DMSO
DFO
CoCl2
HA-PP2AC
CMV-GST-pVHL
GST pull-down
IB: HA-PP2AC
IB: GST-pVHL
WCL
IB: GST-pVHL
IB: HA-PP2AC
IB: HIF2α
C
HA-Akt1
CMV-GST-PP2AC
Flag-pVHL
GST pull-down
IB: HA-Akt1
IB: Flag-pVHL
IB: GST-PP2AC
WCL
IB: HA-Akt1
IB: Flag-pVHL
IB: GST-PP2AC
D
HA-Akt3
CMV-GST-PP2AC
Flag-pVHL
GST pull-down
IB: HA-Akt3
IB: Flag-pVHL
IB: GST-PP2AC
WCL
IB: HA-Akt3
IB: Flag-pVHL
IB: GST-PP2AC
E
sh-Scr
sh-EglN1
CMV-GST-PP2AC
HA-Akt1
GST pull-down
IB: HA-Akt1
IB: GST
WCL
IB: HA-Akt1
IB: GST
F
sh-Scr
sh-EglN1
CMV-GST-PP2AC
HA-Akt3
GST pull-down
IB: HA-Akt3
IB: GST
WCL
IB: HA-Akt3
IB: GST
G
EV
pVHL
786-O
CMV-GST-PP2AC
HA-Akt1
GST pull-down
IB: HA-Akt1
IB: GST-PP2AC
WCL
IB: HA-Akt1
IB: GST-PP2AC
IB: HA-pVHL
H
EV
pVHL
786-O
CMV-GST-PP2AC
HA-Akt3
GST pull-down
IB: HA-Akt3
IB: GST-PP2AC
WCL
IB: HA-Akt3
IB: GST-PP2AC
IB: HA-pVHL
I
EV
WT
P125A
P313A
P125/313A
HA-Akt1
CMV-GST-PP2AC
GST pull-down
IB: HA-Akt1
IB: GST-PP2AC
WCL
IB: HA-Akt1
IB: GST-PP2AC
J
GST pull-down
Input
GST
GST-Akt1
pVHL
IB: pVHL
GST-Akt1
IB: GST
GST
K
PP2AC
GST-Akt1
pVHL
0 4 8 12 0 4 8 12 time (min)
IB: pT308-Akt
IB: Akt-Pro313-OH
IB: GST-Akt1
IB: pVHL
IB: PP2AC
L
Relative pT308-Akt intensity
1.2
1
0.8
0.6
0.4
0.2
0
Ctr
pVHL
0 4 8 12 (min)
M
insulin/EGF
PI3K
PDK1
Akt
T308
EglN1
pVHL
PP2A
PDK1

Fig. S14

pVHL interacts with phosphatase PP2A to promote PP2A-mediated dephosphorylation of Akt at the T308. (A-B) GST pull-down analysis of WCL derived from HEK293 cells transfected with the indicated constructs to illustrate the interaction of the catalytic subunit of PP2A (PP2AC) with pVHL (A), a process that could not be abolished by hypoxia mimetic reagents (B). (C-H) GST pull-down analysis of WCL derived from HEK293 or 786-O cells transfected with the indicated constructs to illustrate that the interaction of PP2AC with Akt1, but not Akt3, can be promoted by pVHL (C-D), and diminished by knockdown of *EglN1* (E-F) or *VHL* deficiency (G-H). (I) GST pull-down analysis of WCL derived from HEK293 cells co-transfected pVHL with WT-Akt1 or various Akt1 mutants harboring a proline to alanine mutation in the identified proline-hydroxylation residues of Akt1. (J) GST-Akt1, purified from HEK293 cells, could pull down recombinant pVHL proteins. GST was used as a negative control. (K-L) *In vitro* dephosphorylation assays were performed with active recombinant PP2A and purified GST-Akt1 in the presence or absence of recombinant pVHL (K). A quantification of the pT308-Akt signal intensity in various lanes was plotted in (L). (M) A proposed model to illustrate a possible role of pVHL in contributing to the oscillation of Akt T308 phosphorylation and kinase activity upon the insulin stimulation. Specifically, EglN1-mediated hydroxylation of Akt facilitates the recruitment of pVHL, which may function as an adaptor protein to further recruit the phosphatase PP2A, the major characterized pT308-Akt phosphatase. In addition, the interaction of proline-hydroxylated species of Akt with pVHL also blocks the interaction of Akt1 with its upstream activating kinase, PDK1, thereby keeping Akt in an inactive state.

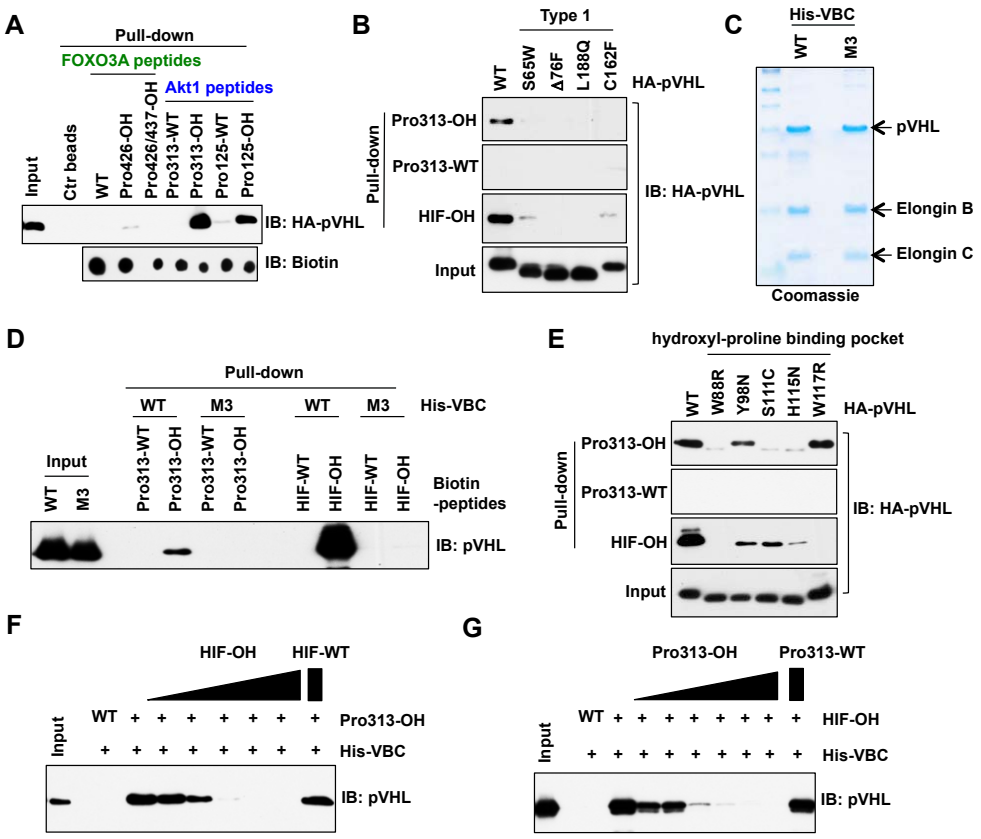

Fig. S15

Synthetic peptides derived from HIF1α and Akt1 compete with one another for binding to pVHL *in vitro* in a proline-hydroxylation-dependent manner. (A) Streptavidin pull-down assays were performed using the indicated biotinylated synthetic FOXO3A- or Akt1-derived peptides and WCL derived from HEK293 cells transfected with HA-pVHL (top panel). Dot immunoblot assays were carried out to illustrate that equal amount of these synthetic peptides were used in each lane (bottom panel). (B, E) Streptavidin pull-down assays were performed using the indicated biotinylated synthetic HIF1α- or Akt1-derived peptides and WCL derived from HEK293 cells transfected with different mutants of HA-pVHL. (C-D) Streptavidin pull-down assays were performed using the indicated biotinylated peptides with bacterially purified pVHL/Elongin B and C complex (VBC) (C) to illustrate that mutating these three critical residues within the pVHL hydroxyl-proline binding pocket compromised the ability of pVHL to recognize hydroxylated HIF1α or Akt1 synthetic peptides (D). M3 indicated the S111G/H115L/W117G mutant form of pVHL. (F-G) *In vitro* synthetic peptides competing assays were carried out with the indicated peptides, with the HIF-WT or Akt1-Pro^{313}-WT peptides as negative control, to illustrate that synthetic peptides derived from HIF1α and Akt1 could efficiently compete with one another to bind bacterially purified recombinant pVHL/Elongin B/C complex *in vitro* in a proline hydroxylation- and dose-dependent manner.

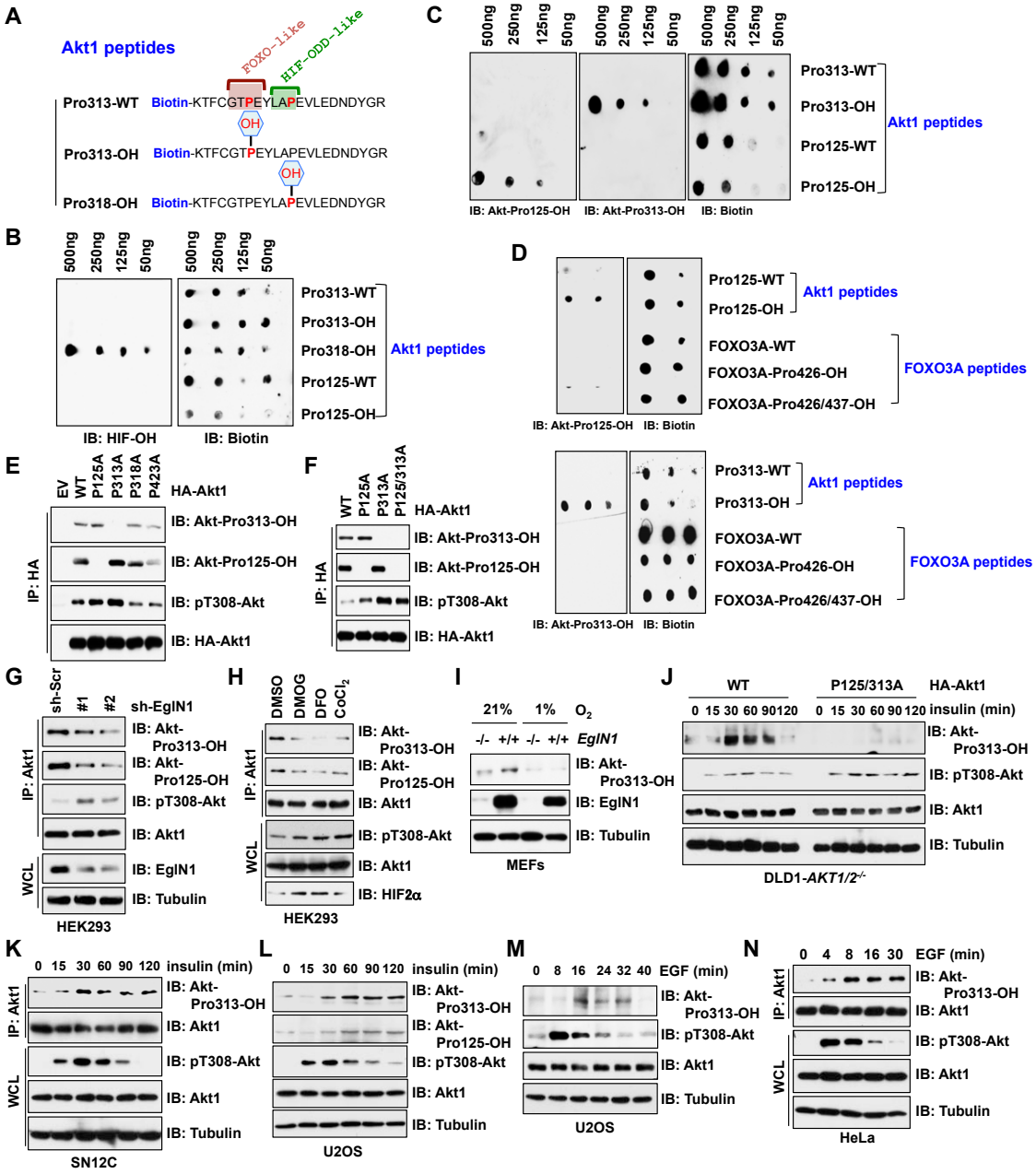
A
Akt1 peptides
FOXO-like
HIF-ODD-like
Pro313-WT Biotin-KTFCGTPEYLAPEVLEDNDYGR
Pro313-OH Biotin-KTFCGTPEYLAPEVLEDNDYGR
Pro318-OH Biotin-KTFCGTPEYLAPEVLEDNDYGR
B
500ng 250ng 125ng 50ng
Pro313-WT
Pro313-OH
Pro318-OH
Pro125-WT
Pro125-OH
Akt1 peptides
IB: HIF-OH
IB: Biotin
C
500ng 250ng 125ng 50ng
Pro313-WT
Pro313-OH
Pro125-WT
Pro125-OH
Akt1 peptides
IB: Akt-Pro125-OH
IB: Akt-Pro313-OH
IB: Biotin
D
Pro125-WT
Pro125-OH
Akt1 peptides
FOXO3A-WT
FOXO3A-Pro426-OH
FOXO3A-Pro426/437-OH
FOXO3A peptides
IB: Akt-Pro125-OH
IB: Biotin
E
EV WT P125A P313A P318A P423A
HA-Akt1
IP: HA
IB: Akt-Pro313-OH
IB: Akt-Pro125-OH
IB: pT308-Akt
IB: HA-Akt1
F
WT P125A P313A P125/313A
HA-Akt1
IP: HA
IB: Akt-Pro313-OH
IB: Akt-Pro125-OH
IB: pT308-Akt
IB: HA-Akt1
Pro313-WT
Pro313-OH
Akt1 peptides
FOXO3A-WT
FOXO3A-Pro426-OH
FOXO3A-Pro426/437-OH
FOXO3A peptides
IB: Akt-Pro313-OH
IB: Biotin
G
sh-Scr #1 #2 sh-EgIN1
IP: Akt1
WCL
IB: Akt-Pro313-OH
IB: Akt-Pro125-OH
IB: pT308-Akt
IB: Akt1
IB: EgIN1
IB: Tubulin
HEK293
H
DMSO DMOG DFO CoCl2
IP: Akt1
WCL
IB: Akt-Pro313-OH
IB: Akt-Pro125-OH
IB: Akt1
IB: pT308-Akt
IB: Akt1
IB: HIF2α
HEK293
I
21% 1% O2
-/- +/+ -/- +/+ EgIN1
IB: Akt-Pro313-OH
IB: EgIN1
IB: Tubulin
MEFs
J
WT P125/313A HA-Akt1
0 15 30 60 90 120 0 15 30 60 90 120 insulin (min)
IB: Akt-Pro313-OH
IB: pT308-Akt
IB: Akt1
IB: Tubulin
DLD1-AKT1/2-/-
K
0 15 30 60 90 120 insulin (min)
IP: Akt1
WCL
IB: Akt-Pro313-OH
IB: Akt1
IB: pT308-Akt
IB: Akt1
IB: Tubulin
SN12C
L
0 15 30 60 90 120 insulin (min)
IB: Akt-Pro313-OH
IB: Akt-Pro125-OH
IB: pT308-Akt
IB: Akt1
IB: Tubulin
U2OS
M
0 8 16 24 32 40 EGF (min)
IB: Akt-Pro313-OH
IB: pT308-Akt
IB: Akt1
IB: Tubulin
U2OS
N
0 4 8 16 30 EGF (min)
IP: Akt1
WCL
IB: Akt-Pro313-OH
IB: Akt1
IB: pT308-Akt
IB: Akt1
IB: Tubulin
HeLa

Fig. S16

Generation and validation of the antibodies specifically recognize hydroxy-Pro^{125} and hydroxy-Pro^{313} of Akt1, respectively. (A) A schematic representation of the various biotinylated synthetic Akt1-derived peptides covering aa307-328 of Akt1. (B) Each indicated synthetic peptides in (A) was diluted and used for dot immunoblot analysis with the well-characterized anti-HIF-OH antibody that specifically recognizes hydroxy-Pro^{564} of HIF1α. (C-D) Dot immunoblot analyses were performed with the indicated biotinylated synthetic peptides diluted with different concentrations, and detected with either anti-Akt1-Pro^{125}-OH or anti-Akt1-Pro^{313}-OH antibody, as indicated. (E-F) IB analysis of IP and WCL derived from HEK293 cells transfected with WT and various mutant forms of Akt1 to illustrate that inactivation of Pro^{125} and/or Pro^{313} specifically abolished the detected hydroxylation events by the anti-Akt1-Pro^{125}-OH or anti-Akt1-Pro^{313}-OH antibody, respectively. (G-H) IB analysis of IP and WCL derived from HEK293 cells with *EglN1* knockdown (G) or treatment with hypoxia mimetic reagents (H) for 16 hrs before harvesting. (I) IB analysis of WCL derived from WT or *EglN1*$^{-/-}$ MEFs that were cultured in the presence (21%) or absence (1%) of oxygen for 16 hrs before harvesting. (J) IB analysis of WCL derived from DLD1-*AKT1/2*$^{-/-}$ cells lentivirally infected with WT- or P125/313A-Akt1. Resulting cells were serum starved for 24 hrs followed by stimulation with insulin (0.1 μM). At the indicated time points, WCL were harvested for IB analysis. (K-N) IB analysis of IP or WCL derived from SN12C, U2OS or HeLa cells serum starved for 24 hrs followed by stimulation with insulin (0.1 μM) or EGF (100 ng/ml). At the indicated time points, WCL were harvested for IB analysis.

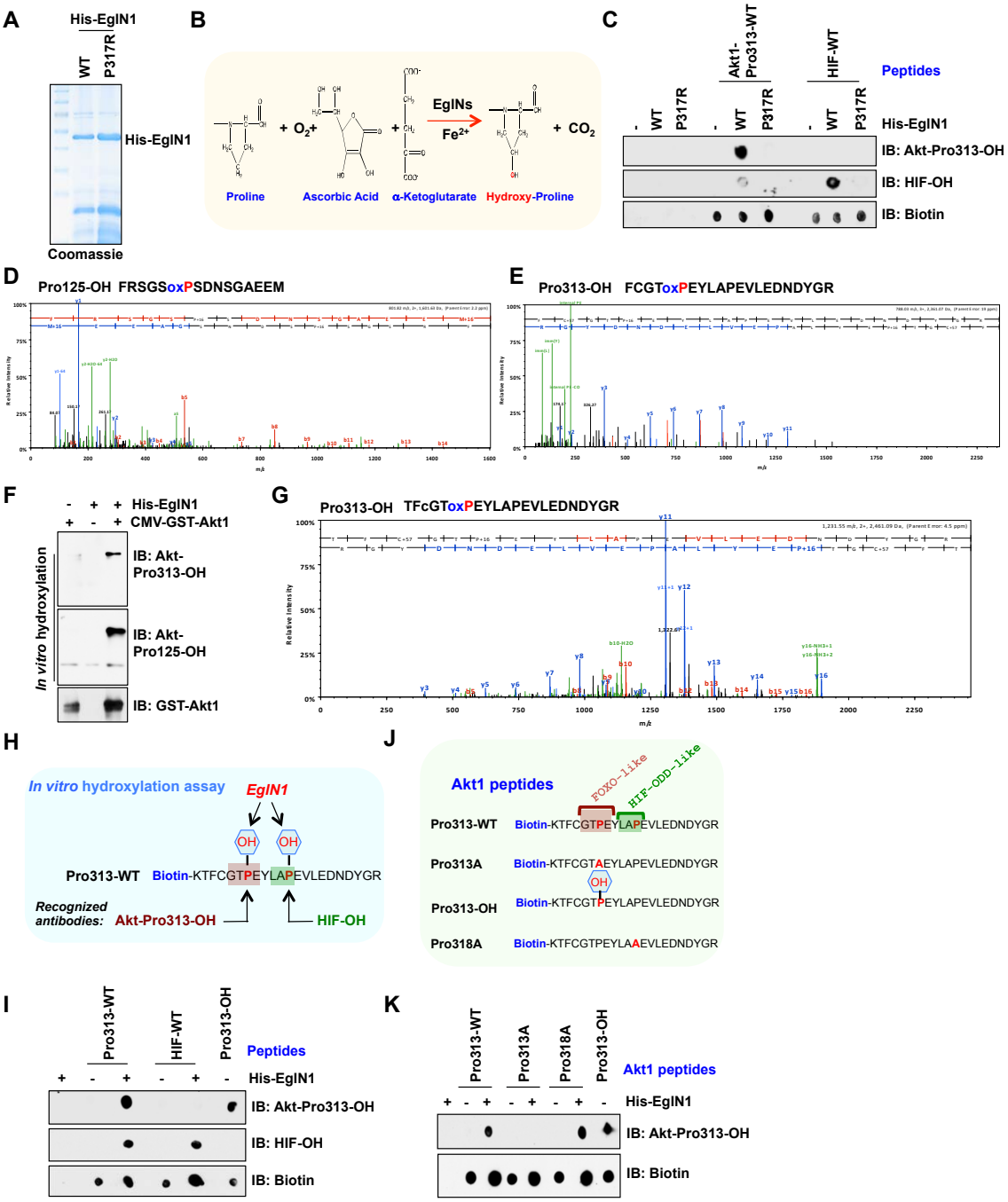
A
His-EglN1
WT
P317R
His-EglN1
Coomassie
B
+ O2+
EglNs
Fe2+
+ CO2
Proline
Ascorbic Acid
α-Ketoglutarate
Hydroxy-Proline
C
Akt1-Pro313-WT
HIF-WT
Peptides
- WT P317R - WT P317R - WT P317R
His-EglN1
IB: Akt-Pro313-OH
IB: HIF-OH
IB: Biotin
D
Pro125-OH FRSGSoxPSDNSGAEEM
E
Pro313-OH FCGToxPEYLAPEVLEDNDYGR
F
- + + His-EglN1
+ - + CMV-GST-Akt1
In vitro hydroxylation
IB: Akt-Pro313-OH
IB: Akt-Pro125-OH
IB: GST-Akt1
G
Pro313-OH TFcGToxPEYLAPEVLEDNDYGR
H
In vitro hydroxylation assay
EglN1
Pro313-WT Biotin-KTFCGTPEYLAPEVLEDNDYGR
Recognized antibodies:
Akt-Pro313-OH
HIF-OH
J
Akt1 peptides
FOXO-like
HIF-ODD-like
Pro313-WT Biotin-KTFCGTPEYLAPEVLEDNDYGR
Pro313A Biotin-KTFCGTAEYLAPEVLEDNDYGR
Pro313-OH Biotin-KTFCGTPEYLAPEVLEDNDYGR
Pro318A Biotin-KTFCGTPEYLAAEVLEDNDYGR
I
Pro313-WT
HIF-WT
Pro313-OH
Peptides
+ - + - + - His-EglN1
IB: Akt-Pro313-OH
IB: HIF-OH
IB: Biotin
K
Pro313-WT
Pro313A
Pro318A
Pro313-OH
Akt1 peptides
+ - + - + - + - His-EglN1
IB: Akt-Pro313-OH
IB: Biotin

Fig. S17

EglN1 hydroxylates Akt1 *in vitro*. (A-C) Coomassie staining of the bacterially purified recombinant WT and catalytic-inactive (P317R) EglN1 (A), which were used for *in vitro* hydroxylation assays (B-C), where HIF1α peptide was used as a positive control. (D) Mass spectrometry analysis to detect the presence of proline hydroxylation event at the Akt1 Pro^{125} site in the reaction products of *in vitro* hydroxylation assays with recombinant His-EglN1 and synthetic Akt1 peptide spanning the Pro^{125} region. *In vitro* hydroxylation products were identified by LC-MS/MS analysis on a Thermo Orbitrap Elite mass spectrometer in positive ion mode and fragmented using higher energy collisional dissociation (HCD). The shift in the b- series ions after **b5** shows that the remaining peptide fragments contain a Pro hydroxylation since they shift by exactly 15.99 Da. The spectrum is dominated by b- series ions generated from the N-terminus rather than y- series ions. (E) LC-MS/MS analysis to detect the presence of proline hydroxylation event at the Pro^{313} site of Akt1 in the reaction products of *in vitro* hydroxylation assays with recombinant His-EglN1 and synthetic Akt1 peptide spanning the Pro^{313} region. The shift in the y- series ions after **y4** shows that the remaining peptide fragments contain a Pro hydroxylation since they shift by exactly 15.99 Da. The spectrum is dominated by y- series ions generated from the C-terminus rather than b- series ions. (F-G) *In vitro* hydroxylation assays were performed with bacterially purified His-EglN1 and GST-Akt1 purified from 293T cells ectopically expressing CMV-GST-Akt1 as substrate. The proline-hydroxylation events at the Pro^{125} and Pro^{313} sites in the resulting enzymatic reaction were analyzed by immunoblot (IB) analysis with the anti-Akt1-Pro^{125}-OH or anti-Akt1-Pro^{313}-OH antibody, respectively (F), and further subjected to LC-MS/MS analysis to further confirm the Pro^{313}-OH event occurring at Akt1 (G). (H) A schematic illustration of the *in vitro* hydroxylated product derived from the synthetic Akt1 peptide, that could be subsequently recognized by the hydroxyl-Proline HIF antibody or the hydroxyl-Pro^{313}-Akt1 antibody, respectively. (I) *In vitro* hydroxylation assays were performed with the indicated biotinylated synthetic Akt1 peptides (H) as substrate. The proline-hydroxylation events at the Pro^{313} and Pro^{318} sites in the resulting enzymatic reaction were analyzed by dot immunoblot analysis with the indicated antibodies (I). (J-K) Various biotinylated synthetic Akt-derived peptides (J) were used for *in vitro* hydroxylation assays as described in (C), and then subjected to dot immunoblot analysis with the anti-Akt1-Pro^{313}-OH antibody to illustrate that mutating Pro^{313}, but not Pro^{318} abolished EglN1-mediated hydroxylation event that could be detected by the anti-Akt1-Pro^{313}-OH antibody (K).

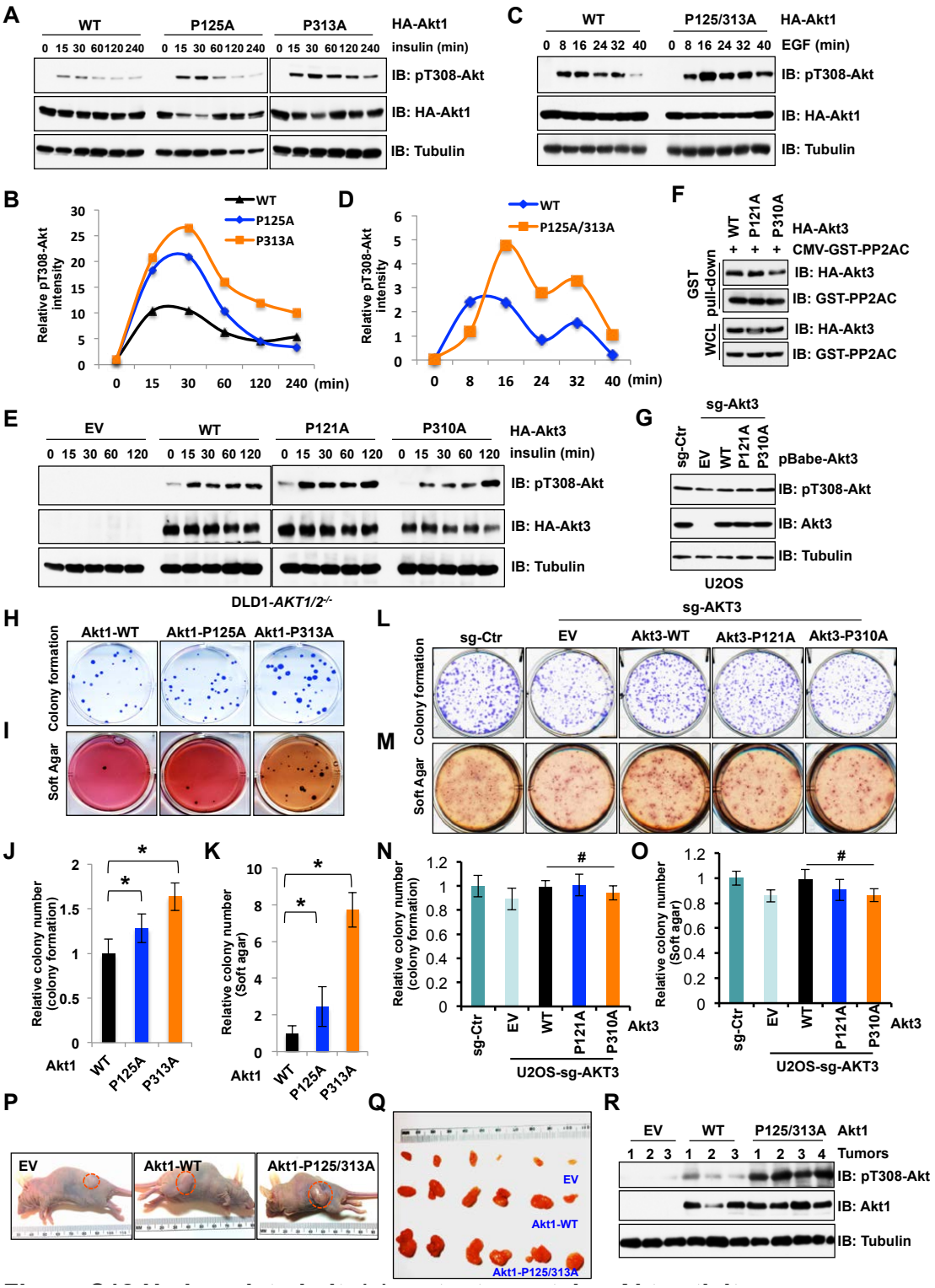
A
WT
P125A
P313A
HA-Akt1
0 15 30 60 120 240
insulin (min)
IB: pT308-Akt
IB: HA-Akt1
IB: Tubulin
C
WT
P125/313A
HA-Akt1
0 8 16 24 32 40
EGF (min)
IB: pT308-Akt
IB: HA-Akt1
IB: Tubulin
B
WT
P125A
P313A
Relative pT308-Akt intensity
0 15 30 60 120 240 (min)
D
WT
P125A/313A
Relative pT308-Akt intensity
0 8 16 24 32 40 (min)
F
WT
P121A
P310A
HA-Akt3
CMV-GST-PP2AC
GST pull-down
WCL
IB: HA-Akt3
IB: GST-PP2AC
IB: HA-Akt3
IB: GST-PP2AC
E
EV
WT
P121A
P310A
HA-Akt3
0 15 30 60 120
insulin (min)
IB: pT308-Akt
IB: HA-Akt3
IB: Tubulin
DLD1-AKT1/2-/-
G
sg-Akt3
sg-Ctr
EV
WT
P121A
P310A
pBabe-Akt3
IB: pT308-Akt
IB: Akt3
IB: Tubulin
U2OS
H
Akt1-WT
Akt1-P125A
Akt1-P313A
Colony formation
I
Soft Agar
L
sg-AKT3
sg-Ctr
EV
Akt3-WT
Akt3-P121A
Akt3-P310A
Colony formation
M
Soft Agar
J
Relative colony number (colony formation)
Akt1
WT
P125A
P313A
K
Relative colony number (Soft agar)
Akt1
WT
P125A
P313A
N
Relative colony number (colony formation)
sg-Ctr
EV
WT
P121A
P310A
Akt3
U2OS-sg-AKT3
O
Relative colony number (Soft agar)
sg-Ctr
EV
WT
P121A
P310A
Akt3
U2OS-sg-AKT3
P
EV
Akt1-WT
Akt1-P125/313A
Q
EV
Akt1-WT
Akt1-P125/313A
R
EV
WT
P125/313A
Akt1
1 2 3 1 2 3 1 2 3 4
Tumors
IB: pT308-Akt
IB: Akt1
IB: Tubulin

Fig. S18

Disruption of proline-hydroxylaiton events at Pro^{125} and Pro^{313} in Akt1, but not the corresponding mutation in Akt3, leads to sustained Akt kinase activity in cells. (A-B) DLD1-*AKT1/2*$^{-/-}$ cells were lentivirally infected with WT-, P125A- or P313A-Akt1 and selected with puromycin (1 μg/ml). Resulting cells were serum starved for 24 hrs followed by stimulation with insulin (0.1 μM). At the indicated time points, WCL were harvested for IB analysis (A). The relative intensity of pT308-Akt as detected by IB analysis in (A) at different time points was quantified in (B). (C-D) DLD1-*AKT1/2*$^{-/-}$ cells were lentivirally infected with WT- or P125/313A-Akt1, and selected with puromycin (1 μg/ml) for 72 hrs. Resulting cells were serum starved for 24 hrs followed by stimulation with EGF (100 ng/ml). At the indicated time points, WCL were harvested for IB analysis (C). The relative intensity of pT308-Akt as detected by IB analysis in (C) at different time points was quantified in (D). (E) IB analysis of WCL derived from DLD1-*AKT1/2*$^{-/-}$ cells infected with retroviral vectors to stably express WT-Akt3 or mutant forms of Akt3 with putative hydroxylated proline being replaced with alanine at the corresponding sites. Resulting cells were serum starved for 24 hrs followed by stimulation with insulin (0.1 μM). At the indicated time points, WCL were harvested for IB analysis. (F) GST pull-down assays to demonstrate that GST-PP2AC purified from mammalian cells ectopically expressing CMV-GST-PP2AC interacts with the indicated mutant Akt3 in HEK293 cells. (G) Wild type and mutant forms of Akt3 were re-introduced into CRISPR-mediated *AKT3*-knockout (sg-Akt3) U2OS cells to examine the effects of mutating the corresponding Proline residues in Akt3 towards Akt activity in cells. (H-K) Colony formation (H) and soft agar (I) assays were carried out with various cell lines generated in (A). Relative colony numbers for colony formation (J) and soft agar (K) assays were further quantified (mean±SD, n=3 wells/group). $*P < 0.05$ (*t* test). (L-O) Colony formation (L) and soft agar (M) assays were carried out with various cell lines generated in (G). Relative colony numbers for colony formation (N) and soft agar (O) were further quantified (mean±SD, n=3 wells/group). $^{\#}P > 0.05$ (*t* test). (P-R) Xenograft mouse assays were performed with the cell lines generated in (C). Tumor size was monitored (P), and tumors were dissected after euthanizing the mice (Q). The phosphorylation status of Akt1 (pT308-Akt) was detected with IB analysis of WCL derived from recovered tumors (R).

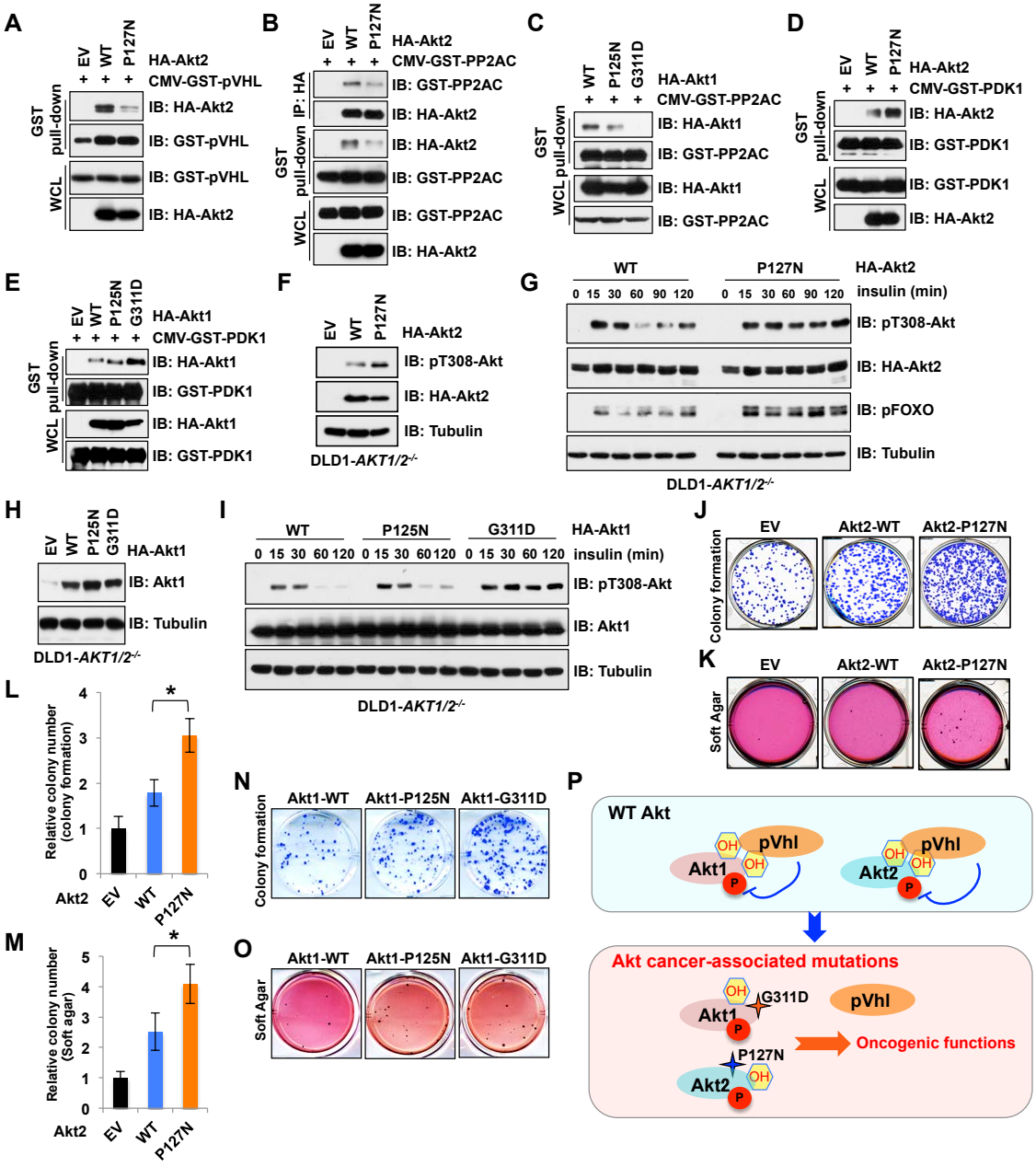
A
EV
WT
P127N
HA-Akt2
CMV-GST-pVHL
GST pull-down
IB: HA-Akt2
IB: GST-pVHL
WCL
IB: GST-pVHL
IB: HA-Akt2
B
HA-Akt2
CMV-GST-PP2AC
IP: HA
IB: GST-PP2AC
IB: HA-Akt2
GST pull-down
IB: HA-Akt2
IB: GST-PP2AC
WCL
IB: GST-PP2AC
IB: HA-Akt2
C
WT
P125N
G311D
HA-Akt1
CMV-GST-PP2AC
GST pull-down
IB: HA-Akt1
IB: GST-PP2AC
WCL
IB: HA-Akt1
IB: GST-PP2AC
D
HA-Akt2
CMV-GST-PDK1
GST pull-down
IB: HA-Akt2
IB: GST-PDK1
WCL
IB: GST-PDK1
IB: HA-Akt2
E
EV
WT
P125N
G311D
HA-Akt1
CMV-GST-PDK1
GST pull-down
IB: HA-Akt1
IB: GST-PDK1
WCL
IB: HA-Akt1
IB: GST-PDK1
F
EV
WT
P127N
HA-Akt2
IB: pT308-Akt
IB: HA-Akt2
IB: Tubulin
DLD1-AKT1/2-/-
G
WT
P127N
HA-Akt2
0 15 30 60 90 120
0 15 30 60 90 120
insulin (min)
IB: pT308-Akt
IB: HA-Akt2
IB: pFOXO
IB: Tubulin
DLD1-AKT1/2-/-
H
EV
WT
P125N
G311D
HA-Akt1
IB: Akt1
IB: Tubulin
DLD1-AKT1/2-/-
I
WT
P125N
G311D
HA-Akt1
0 15 30 60 120 0 15 30 60 120 0 15 30 60 120
insulin (min)
IB: pT308-Akt
IB: Akt1
IB: Tubulin
DLD1-AKT1/2-/-
J
EV
Akt2-WT
Akt2-P127N
Colony formation
K
EV
Akt2-WT
Akt2-P127N
Soft Agar
L
Relative colony number (colony formation)
0
1
2
3
4
*
Akt2
EV
WT
P127N
M
Relative colony number (Soft agar)
0
1
2
3
4
5
*
Akt2
EV
WT
P127N
N
Akt1-WT
Akt1-P125N
Akt1-G311D
Colony formation
O
Akt1-WT
Akt1-P125N
Akt1-G311D
Soft Agar
P
WT Akt
pVhl
Akt1
Akt2
OH
P
Akt cancer-associated mutations
G311D
P127N
pVhl
Akt1
Akt2
Oncogenic functions

Fig. S19

Cancer-associated mutations in Akt promote Akt kinase activity and oncogenic functions. (A-E) GST pull-down assays to demonstrate that cancer-derived Akt mutations reduced Akt interaction with pVHL and PP2AC, but elevated Akt interaction with PDK1 in HEK293 cells. (F-I) IB analysis of WCL derived from DLD1-*AKT1/2*$^{-/-}$ cells infected with retroviral vectors to stably express WT-Akt1 or Akt2, cancer-associated mutant form of P127N-Akt2 (F) or G311D-Akt1 (H) at comparable levels. Infected cells were selected with hygromycin (200 μg/ml) for 72 hrs to eliminate non-infected cells. Resulting cells were serum starved for 24 hrs followed by stimulation with insulin (0.1 μM). At the indicated time points, WCL were harvested for IB analysis (G and I). (J-O) Cell lines generated in (F and H) were used to perform colony formation (J and N) and soft agar assays (K and O). Relative colony numbers for colony formation (L) and soft agar assays (M) were further quantified (mean±SD, n=3 wells/group). **P* < 0.05 (*t* test). (P) A schematic representation of biological consequences of how the VHL/EGLN1 signaling axis suppresses tumorigenesis in part by suppressing the Akt oncogenic signaling pathway. Specifically, pVHL interacts with, and suppresses the proline-hydroxylated species of Akt1 and Akt2. Pathologically, cancer patient-associated mutations in Akt1 or Akt2 (G311D and P127N) may impair pVHL-mediated suppression of Akt to favor tumorigenesis (bottom panel).

References and Notes

1. F. Chen, T. Kishida, M. Yao, T. Hustad, D. Glavac, M. Dean, J. R. Gnarra, M. L. Orcutt, F. M. Duh, G. Glenn, J. Green, Y. E. Hsia, J. Lamiell, H. Li, M. H. Wei, L. Schmidt, K. Tory, I. Kuzmin, T. Stackhouse, F. Latif, W. M. Linehan, M. Lerman, B. Zbar, Germline mutations in the von Hippel-Lindau disease tumor suppressor gene: Correlations with phenotype. *Hum. Mutat.* **5**, 66–75 (1995). Medline doi:10.1002/humu.1380050109

2. L. Gossage, T. Eisen, E. R. Maher, VHL, the story of a tumour suppressor gene. *Nat. Rev. Cancer* **15**, 55–64 (2015). Medline doi:10.1038/nrc3844

3. W. Y. Kim, W. G. Kaelin, Role of VHL gene mutation in human cancer. *J. Clin. Oncol.* **22**, 4991–5004 (2004). Medline doi:10.1200/JCO.2004.05.061

4. G. V. Thomas, C. Tran, I. K. Mellinghoff, D. S. Welsbie, E. Chan, B. Fueger, J. Czernin, C. L. Sawyers, Hypoxia-inducible factor determines sensitivity to inhibitors of mTOR in kidney cancer. *Nat. Med.* **12**, 122–127 (2006). Medline doi:10.1038/nm1337

5. G. Hudes, M. Carducci, P. Tomczak, J. Dutcher, R. Figlin, A. Kapoor, E. Staroslawska, J. Sosman, D. McDermott, I. Bodrogi, Z. Kovacevic, V. Lesovoy, I. G. Schmidt-Wolf, O. Barbarash, E. Gokmen, T. O'Toole, S. Lustgarten, L. Moore, R. J. Motzer, Global ARCC Trial, Temsirolimus, interferon alfa, or both for advanced renal-cell carcinoma. *N. Engl. J. Med.* **356**, 2271–2281 (2007). Medline doi:10.1056/NEJMoa066838

6. J. B. Brugarolas, F. Vazquez, A. Reddy, W. R. Sellers, W. G. Kaelin Jr., TSC2 regulates VEGF through mTOR-dependent and -independent pathways. *Cancer Cell* **4**, 147–158 (2003). Medline doi:10.1016/S1535-6108(03)00187-9

7. M. Laplante, D. M. Sabatini, mTOR signaling in growth control and disease. *Cell* **149**, 274–293 (2012). Medline doi:10.1016/j.cell.2012.03.017

8. M. Hager, H. Haufe, R. Kemmerling, W. Hitzl, G. Mikuz, P. L. Moser, C. Kolbitsch, Increased activated Akt expression in renal cell carcinomas and prognosis. *J. Cell. Mol. Med.* **13** (8B), 2181–2188 (2009). Medline doi:10.1111/j.1582-4934.2008.00488.x

9. A. P. Young, S. Schlisio, Y. A. Minamishima, Q. Zhang, L. Li, C. Grisanzio, S. Signoretti, W. G. Kaelin Jr., VHL loss actuates a HIF-independent senescence programme mediated by Rb and p400. *Nat. Cell Biol.* **10**, 361–369 (2008). Medline doi:10.1038/ncb1699

10. M. Aoki, O. Batista, A. Bellacosa, P. Tsichlis, P. K. Vogt, The akt kinase: Molecular determinants of oncogenicity. *Proc. Natl. Acad. Sci. U.S.A.* **95**, 14950–14955 (1998). Medline doi:10.1073/pnas.95.25.14950

11. E. Maltepe, J. V. Schmidt, D. Baunoch, C. A. Bradfield, M. C. Simon, Abnormal angiogenesis and responses to glucose and oxygen deprivation in mice lacking the protein ARNT. *Nature* **386**, 403–407 (1997). Medline doi:10.1038/386403a0

12. P. H. Maxwell, M. S. Wiesener, G. W. Chang, S. C. Clifford, E. C. Vaux, M. E. Cockman, C. C. Wykoff, C. W. Pugh, E. R. Maher, P. J. Ratcliffe, The tumour suppressor protein VHL targets hypoxia-inducible factors for oxygen-dependent proteolysis. *Nature* **399**, 271–275 (1999). Medline doi:10.1038/20459

13. J. H. Min, H. Yang, M. Ivan, F. Gertler, W. G. Kaelin Jr., N. P. Pavletich, Structure of an HIF-1alpha -pVHL complex: Hydroxyproline recognition in signaling. *Science* **296**, 1886–1889 (2002). Medline doi:10.1126/science.1073440

14. K. M. Lonergan, O. Iliopoulos, M. Ohh, T. Kamura, R. C. Conaway, J. W. Conaway, W. G. Kaelin Jr., Regulation of hypoxia-inducible mRNAs by the von Hippel-Lindau tumor suppressor protein requires binding to complexes containing elongins B/C and Cul2. *Mol. Cell. Biol.* **18**, 732–741 (1998). Medline doi:10.1128/MCB.18.2.732

15. M. Ohh, C. W. Park, M. Ivan, M. A. Hoffman, T. Y. Kim, L. E. Huang, N. Pavletich, V. Chau, W. G. Kaelin, Ubiquitination of hypoxia-inducible factor requires direct binding to the beta-domain of the von Hippel-Lindau protein. *Nat. Cell Biol.* **2**, 423–427 (2000). Medline doi:10.1038/35017054

16. L. Li, L. Zhang, X. Zhang, Q. Yan, Y. A. Minamishima, A. F. Olumi, M. Mao, S. Bartz, W. G. Kaelin Jr., Hypoxia-inducible factor linked to differential kidney cancer risk seen with type 2A and type 2B VHL mutations. *Mol. Cell. Biol.* **27**, 5381–5392 (2007). Medline doi:10.1128/MCB.00282-07

17. W. C. Hon, M. I. Wilson, K. Harlos, T. D. Claridge, C. J. Schofield, C. W. Pugh, P. H. Maxwell, P. J. Ratcliffe, D. I. Stuart, E. Y. Jones, Structural basis for the recognition of hydroxyproline in HIF-1 alpha by pVHL. *Nature* **417**, 975–978 (2002). Medline doi:10.1038/nature00767

18. M. Ivan, K. Kondo, H. Yang, W. Kim, J. Valiando, M. Ohh, A. Salic, J. M. Asara, W. S. Lane, W. G. Kaelin Jr., HIFalpha targeted for VHL-mediated destruction by proline hydroxylation: Implications for O_2 sensing. *Science* **292**, 464–468 (2001). Medline doi:10.1126/science.1059817

19. P. Jaakkola, D. R. Mole, Y.-M. Tian, M. I. Wilson, J. Gielbert, S. J. Gaskell, A. von Kriegsheim, H. F. Hebestreit, M. Mukherji, C. J. Schofield, P. H. Maxwell, C. W. Pugh, P. J. Ratcliffe, Targeting of HIF-α to the von Hippel-Lindau ubiquitylation complex by O_2-regulated prolyl hydroxylation. *Science* **292**, 468–472 (2001). Medline doi:10.1126/science.1059796

20. F. Yu, S. B. White, Q. Zhao, F. S. Lee, HIF-1α binding to VHL is regulated by stimulus-sensitive proline hydroxylation. *Proc. Natl. Acad. Sci. U.S.A.* **98**, 9630–9635 (2001). Medline doi:10.1073/pnas.181341498

21. H. Zhang, P. Gao, R. Fukuda, G. Kumar, B. Krishnamachary, K. I. Zeller, C. V. Dang, G. L. Semenza, HIF-1 inhibits mitochondrial biogenesis and cellular respiration in VHL-deficient renal cell carcinoma by repression of C-MYC activity. *Cancer Cell* **11**, 407–420 (2007). Medline doi:10.1016/j.ccr.2007.04.001

22. D. Huang, T. Li, X. Li, L. Zhang, L. Sun, X. He, X. Zhong, D. Jia, L. Song, G. L. Semenza, P. Gao, H. Zhang, HIF-1-mediated suppression of acyl-CoA dehydrogenases and fatty acid oxidation is critical for cancer progression. *Cell Reports* **8**, 1930–1942 (2014). Medline doi:10.1016/j.celrep.2014.08.028

23. J. D. Carpten, A. L. Faber, C. Horn, G. P. Donoho, S. L. Briggs, C. M. Robbins, G. Hostetter, S. Boguslawski, T. Y. Moses, S. Savage, M. Uhlik, A. Lin, J. Du, Y. W. Qian, D. J. Zeckner, G. Tucker-Kellogg, J. Touchman, K. Patel, S. Mousses, M. Bittner, R. Schevitz,

M. H. Lai, K. L. Blanchard, J. E. Thomas, A transforming mutation in the pleckstrin homology domain of AKT1 in cancer. *Nature* **448**, 439–444 (2007). Medline doi:10.1038/nature05933

24. W. Luo, H. Hu, R. Chang, J. Zhong, M. Knabel, R. O'Meally, R. N. Cole, A. Pandey, G. L. Semenza, Pyruvate kinase M2 is a PHD3-stimulated coactivator for hypoxia-inducible factor 1. *Cell* **145**, 732–744 (2011). Medline doi:10.1016/j.cell.2011.03.054

25. X. Zheng, B. Zhai, P. Koivunen, S. J. Shin, G. Lu, J. Liu, C. Geisen, A. A. Chakraborty, J. J. Moslehi, D. M. Smalley, X. Wei, X. Chen, Z. Chen, J. M. Beres, J. Zhang, J. L. Tsao, M. C. Brenner, Y. Zhang, C. Fan, R. A. DePinho, J. Paik, S. P. Gygi, W. G. Kaelin Jr., Q. Zhang, Prolyl hydroxylation by EglN2 destabilizes FOXO3a by blocking its interaction with the USP9x deubiquitinase. *Genes Dev.* **28**, 1429–1444 (2014). Medline doi:10.1101/gad.242131.114

26. J. Li, Y. Ning, W. Hedley, B. Saunders, Y. Chen, N. Tindill, T. Hannay, S. Subramaniam, The Molecule Pages database. *Nature* **420**, 716–717 (2002). Medline doi:10.1038/nature01307

27. T. A. Millward, S. Zolnierowicz, B. A. Hemmings, Regulation of protein kinase cascades by protein phosphatase 2A. *Trends Biochem. Sci.* **24**, 186–191 (1999). Medline doi:10.1016/S0968-0004(99)01375-4

28. J. H. Zhang, R. C. Qi, T. Chen, T. D. Chung, A. M. Stern, G. F. Hollis, R. A. Copeland, K. R. Oldenburg, Development of a carbon dioxide-capture assay in microtiter plate for aspartyl-β-hydroxylase. *Anal. Biochem.* **271**, 137–142 (1999). Medline doi:10.1006/abio.1999.4135

29. E. Cerami, J. Gao, U. Dogrusoz, B. E. Gross, S. O. Sumer, B. A. Aksoy, A. Jacobsen, C. J. Byrne, M. L. Heuer, E. Larsson, Y. Antipin, B. Reva, A. P. Goldberg, C. Sander, N. Schultz, The cBio cancer genomics portal: An open platform for exploring multidimensional cancer genomics data. *Cancer Discov.* **2**, 401–404 (2012). Medline doi:10.1158/2159-8290.CD-12-0095

30. B. Gan, C. Lim, G. Chu, S. Hua, Z. Ding, M. Collins, J. Hu, S. Jiang, E. Fletcher-Sananikone, L. Zhuang, M. Chang, H. Zheng, Y. A. Wang, D. J. Kwiatkowski, W. G. Kaelin Jr., S. Signoretti, R. A. DePinho, FoxOs enforce a progression checkpoint to constrain mTORC1-activated renal tumorigenesis. *Cancer Cell* **18**, 472–484 (2010). Medline doi:10.1016/j.ccr.2010.10.019

31. Y. A. Minamishima, J. Moslehi, R. F. Padera, R. T. Bronson, R. Liao, W. G. Kaelin Jr., A feedback loop involving the Phd3 prolyl hydroxylase tunes the mammalian hypoxic response in vivo. *Mol. Cell. Biol.* **29**, 5729–5741 (2009). Medline doi:10.1128/MCB.00331-09

32. D. Gao, H. Inuzuka, A. Tseng, R. Y. Chin, A. Toker, W. Wei, Phosphorylation by Akt1 promotes cytoplasmic localization of Skp2 and impairs APCCdh1-mediated Skp2 destruction. *Nat. Cell Biol.* **11**, 397–408 (2009). Medline doi:10.1038/ncb1847

33. P. Liu, W. Gan, H. Inuzuka, A. S. Lazorchak, D. Gao, O. Arojo, D. Liu, L. Wan, B. Zhai, Y. Yu, M. Yuan, B. M. Kim, S. Shaik, S. Menon, S. P. Gygi, T. H. Lee, J. M. Asara, B. D. Manning, J. Blenis, B. Su, W. Wei, Sin1 phosphorylation impairs mTORC2 complex

integrity and inhibits downstream Akt signalling to suppress tumorigenesis. *Nat. Cell Biol.* **15**, 1340–1350 (2013). Medline doi:10.1038/ncb2860

34. Q. Zhang, J. Gu, L. Li, J. Liu, B. Luo, H. W. Cheung, J. S. Boehm, M. Ni, C. Geisen, D. E. Root, K. Polyak, M. Brown, A. L. Richardson, W. C. Hahn, W. G. Kaelin Jr., A. Bommi-Reddy, Control of cyclin D1 and breast tumorigenesis by the EglN2 prolyl hydroxylase. *Cancer Cell* **16**, 413–424 (2009). Medline doi:10.1016/j.ccr.2009.09.029

35. P. Liu, M. Begley, W. Michowski, H. Inuzuka, M. Ginzberg, D. Gao, P. Tsou, W. Gan, A. Papa, B. M. Kim, L. Wan, A. Singh, B. Zhai, M. Yuan, Z. Wang, S. P. Gygi, T. H. Lee, K. P. Lu, A. Toker, P. P. Pandolfi, J. M. Asara, M. W. Kirschner, P. Sicinski, L. Cantley, W. Wei, Cell-cycle-regulated activation of Akt kinase by phosphorylation at its carboxyl terminus. *Nature* **508**, 541–545 (2014). Medline doi:10.1038/nature13079

36. L. Cong, F. Zhang, Genome engineering using CRISPR-Cas9 system. *Methods Mol. Biol.* **1239**, 197–217 (2015). Medline doi:10.1007/978-1-4939-1862-1_10

37. D. Gao, L. Wan, H. Inuzuka, A. H. Berg, A. Tseng, B. Zhai, S. Shaik, E. Bennett, A. E. Tron, J. A. Gasser, A. Lau, S. P. Gygi, J. W. Harper, J. A. DeCaprio, A. Toker, W. Wei, Rictor forms a complex with Cullin-1 to promote SGK1 ubiquitination and destruction. *Mol. Cell* **39**, 797–808 (2010). Medline doi:10.1016/j.molcel.2010.08.016

38. S. B. Breitkopf, M. Yuan, K. P. Helenius, C. A. Lyssiotis, J. M. Asara, Triomics Analysis of Imatinib-Treated Myeloma Cells Connects Kinase Inhibition to RNA Processing and Decreased Lipid Biosynthesis. *Anal. Chem.* **87**, 10995–11006 (2015). Medline doi:10.1021/acs.analchem.5b03040